Wind Energ. Sci., 11, 1429–1460, 2026
https://doi.org/10.5194/wes-11-1429-2026

eawe european academy of wind energy
Open Access WIND ENERGY SCIENCE

Reference floating wind array designs for three representative regions

Leah H. Sirkis, Ericka Lozon, and Matthew Hall

National Laboratory of the Rockies, 15013 Denver West Parkway, Golden, CO 80401, USA

Correspondence: Leah H. Sirkis (leah.sirkis@nlr.gov)

Received: 10 October 2025 – Discussion started: 20 October 2025
Revised: 4 February 2026 – Accepted: 5 March 2026 – Published: 28 April 2026

Abstract. This work presents the systematic development of three open-source reference floating wind array designs. The designs are tailored to representative site conditions for three regions of the United States: Humboldt Bay off the coast of California, the Gulf of Maine, and the Gulf of America. We adopted existing reference designs for the individual 15 MW turbines, semisubmersible floating platforms, substations, mooring systems, and power cables – integrating and adapting them as needed for each location. We adapted existing dynamic cable designs to use larger conductor sizes to meet the arrays' power transmission requirements, and we set up redundant mooring systems for each substation. The layout of each array is a uniform-grid design optimized to approximately minimize the levelized cost of energy (LCOE) within a square lease area while satisfying spatial constraints. These constraints ensure adequate clearances between adjacent turbines and between underwater components during the layout optimization to prevent clashing and ensure that all components reside within the lease boundaries. Substations are included to allow accounting for intra-array cable costs. They are placed within the uniform grid to maintain the navigability of the arrays. For each feasible layout considered, annual energy production and cable routing costs are calculated and updated in the LCOE objective function. After the optimization, we refined the cable routing with a mix of algorithmic and manual methods to ensure that the cables avoid mooring system components and approach the substation with adequate clearances. We confirmed the suitability of each reference array's layout by comparing the wake losses at each wind heading angle to the wind rose, observing that the optimized layouts largely avoid wake losses in the predominant wind directions. These reference arrays provide open-source baseline designs to enable future research and innovation of floating wind technology at the array scale.

1 Introduction

Floating wind turbines can access strong and consistent wind resources while also positioning wind farms farther from shore, reducing visual impacts and conflicts with other ocean co-users; however, floating wind is still a developing technology, and there are no existing large-scale floating wind arrays. The largest floating wind array, Hywind Tampen, has 11 turbines with a combined capacity of 94.6 MW, whereas fixed-bottom wind farms have advanced to gigawatts of capacity. Floating wind array design has only recently become an area of significant research.

Reference designs – open-source definitions of representative systems – have helped floating wind research and development by giving researchers a common starting point and baseline for comparison. Research at the single-turbine level has produced various reference designs at increasing sizes as turbine technology advances over time. The earliest widely

used examples are the National Laboratory of the Rockies (NLR) 5 MW reference wind turbine (Jonkman et al., 2009) and the Offshore Code Comparison Collaboration (OC3)-Hywind spar-buoy reference platform (Jonkman, 2010). Another widely used reference floating platform developed for the 5 MW turbine is the Offshore Code Comparison Collaboration Continuation (OC4)-DeepCWind semisubmersible (Robertson et al., 2014). Both floating system reference designs also include definitions of the tower, control system, and catenary chain mooring system. Reference turbine capacity increased with the Technical University of Denmark 10 MW reference wind turbine (Bak et al., 2013), which was used in research on a range of floating platforms, including public semisubmersible designs in the LIFES50+ project (Yu et al., 2018). The INO WINDMOOR base case reference wind turbine system (Silva de Souza et al., 2021) – including a turbine, semisubmersible floating platform, and mooring system – was developed with a capacity of 12 MW.

The most widely used reference floating system at present is the International Energy Agency (IEA) Wind Technology Collaboration Programme (IEA Wind) 15 MW reference wind turbine (Gaertner et al., 2020) and the University of Maine (UMaine) VolturnUS-S semisubmersible floating platform (Allen et al., 2020). Several other floating platform designs were developed to work with the IEA Wind 15 MW reference turbine as well, including the Windcrete spar and the ActiveFloat semisubmersible reference designs (Mahfouz, 2020). All three of these support structure reference designs were developed with a chain catenary mooring system. In recent years, larger reference wind turbines have been developed, such as the IEA Wind 22 MW reference turbine (Zahle et al., 2024), which includes a semisubmersible design based on the UMaine VolturnUS-S semisubmersible but is tailored to fit the 22 MW turbine.

In general, considerations for underwater components – such as moorings, dynamic cables, and anchors – were limited in the aforementioned reference systems. The mooring systems were basic catenary designs with uniform lengths of chain. Anchors and dynamic power cables were rarely specified. More complete underwater component reference designs have been developed in recent years. Janocha et al. (2024) developed reference power cable design definitions for floating wind systems, including a set of reference cable properties. Lozon et al. (2025) designed mooring and dynamic power cable reference designs for shallow, moderate, and deep water for three representative locations in the United States, including catenary, semitaut, and taut mooring configurations; however, reference definitions of floating wind arrays consisting of multiple floating wind turbines and their associated underwater components have not yet been published.

To aid floating wind research at the array level, there is a need for reference floating array designs comprising mooring systems, dynamic power cables, static cable routing, and the full layout of these items in the array. Reference designs serve future research by providing a baseline and starting point for further exploration.

Previous studies have developed several fixed-bottom reference wind farm designs. The Norwegian Research Centre for Offshore Wind Technology reference wind farm developed a 1.2 GW fixed-bottom uniform-grid array design based on the Dogger Bank Creyke Beck A sizing and location (Kirkeby and Tande, 2014). The reference farm included cable routing and a study on the use of 33 kV versus 66 kV collector systems. The Norwegian Centre for Offshore Wind Energy developed a uniform grid and an irregular (nongridded) 0.8 GW reference fixed-bottom wind farm for conditions in the North Sea (Bak et al., 2017), including cable layouts, operations and maintenance activities, and cost analyses. The IEA Wind Task 55 project developed a set of reference fixed-bottom wind farm arrays based on the Borssele III and IV lease areas off the coast of Belgium and the Netherlands, where they optimized a uniform-grid array layout and an irregular array layout (Kainz et al., 2024). The IEA Wind Task 55 reference farm included cable routing and conductor sizing, and the layout optimization accounted for the water depth of the site. There are currently no floating open-source reference wind array designs to the authors' knowledge, representing a significant gap in floating wind research.

To develop floating wind reference arrays, layout optimization methodologies specific to floating systems are needed. Floating farm layouts require a wide variety of considerations to ensure a feasible and holistic design, including the design and constraints of components that are specific to floating wind, array layout optimization, and intra-array cable routing. Considering all these factors in a floating wind farm layout optimization represents a significant challenge. Mooring systems for floating wind farms – which often have a large, site-specific footprint – must fully reside within the lease area boundaries; therefore, floating array layout optimization must consider the spatial constraints for mooring design and orientation. Varied bathymetry and sediment in the array can also affect the design of specific mooring lines, anchors, and dynamic cables, which can affect the overall costs and mooring footprints. Moorings, platforms, and cables must also not clash with each other. Further considerations for navigability, installation, operations and maintenance, and supply chain availability can also factor into the feasibility of a floating wind layout.

Floating wind layout optimization techniques require an optimization algorithm, an objective function, and floating-specific constraints. There are a variety of optimization algorithms, and research has not yet converged on a specific algorithm to best optimize wind farm layouts. A comparison of optimization algorithms for fixed-bottom wind farm layouts revealed that various different techniques produced similar levelized costs of energy (LCOEs) (Thomas et al., 2023).

The development of constraints and objective functions for floating wind layout optimization has been approached with a variety of priorities and considerations using a wide

range of optimization algorithms. Lerch et al. (2021) used particle swarm optimization to optimize the electrical layout of a floating wind farm for LCOE. Eikrem et al. (2023) used an ensemble optimization method, a form of stochastic optimization that uses an ensemble of controls to approximate a gradient, which is often used in oil reservoir optimization problems. Though ensemble methods often cannot handle constraints, they include them by breaking the problem into subproblems that apply penalty functions to optimize a floating wind farm layout for LCOE and annual energy production (AEP) using a minimum spanning tree algorithm to determine the intra-array cable layout. Rapha (2023) developed an optimization technique for floating wind layouts that algorithmically adjusted the moorings and cables based on bathymetry to account for their changing spatial footprints and costs. Mahfouz et al. (2024) considered the mooring design for wake steering in the layout optimization process. Heitanen et al. (2024) developed a layout optimization tool that included a binary anchor choice based on the soil type and added buffer zones along the mooring lines. The tool maximizes the net present value with a random search optimization algorithm, specifically modeling costs that are affected by the layout of the array. Hall et al. (2024a) developed a layout optimization approach that included anchor selection based on the soil type and mooring adjustment for bathymetry. They used a sequential least-squares gradient-based optimization algorithm. This tool was further developed by Sirkis et al. (2025) to add intra-array cable routing and sizing with a minimum spanning tree algorithm and anchor sizing. They used a particle swarm optimization and a sequential least-squares gradient-based optimization algorithm.

In this paper, we develop reference floating wind array designs for three regions in the United States: Humboldt Bay, the Gulf of Maine, and the Gulf of America. We directly use the mooring and dynamic cable designs developed in Lozon et al. (2025) for these same regions in complete gigawatt-scale array designs. We approximately optimize each array layout with an approach that builds on the layout optimization tool developed in Hall et al. (2024a) and Sirkis et al. (2025) to include novel cable routing techniques and improved layout optimization methods. These array designs will serve as some of the first open-source reference floating array designs, with fully shared design details to facilitate future use and application. The full definition files for these designs are available on GitHub at https://github.com/FloatingArrayDesign/ReferenceDesigns (last access: 16 March 2026).

The layout of this paper is as follows: Sect. 2 describes the general array design process methodology; Sect. 3 defines the component and array designs for Humboldt Bay, the Gulf of Maine, and the Gulf of America, respectively; and, finally, Sect. 4 describes conclusions and future work.

2 Array design methodology

The floating wind array design methodology presented in this paper builds on the techniques in Hall et al. (2024a) and Sirkis et al. (2025) to include improvements to the layout optimization approach and cable routing techniques. We applied the same array design methodology to the development of a reference array design for each of three United States regions. The overall reference array design process, shown in Fig. 1, can be described in six general steps:

1. site parameter selection
2. component type selection
3. component design optimization
4. intra-array cable design
5. layout optimization
6. cable routing adjustment.

We based the site parameter selection on the three reference site condition sets developed in Biglu et al. (2024a) based in Humboldt Bay, the Gulf of Maine, and the Gulf of America. These reference site definitions include meteorological ocean (metocean) characteristics for extreme and fatigue load analysis as well as bathymetry and soil type information representative of several United States regions. Component type selection and design optimization were completed in Lozon et al. (2025). That work used reference metocean, depth, and soil parameters based on Biglu et al. (2024a). The depth and soil information informed the anchor type, the mooring configuration, and the cable type selections. These components were then optimized to minimize cost and meet critical constraints for these conditions.

The present work builds on the site conditions and component designs from previous work to create full floating wind array designs. We select cable conductor sizes needed to meet power requirements for an initial layout and cable routing of a 1 GW farm. We adapt the 300 mm^2 dynamic cable designs from Lozon et al. (2025) for the selected conductor sizes and ensure that they still satisfy the design constraints. We then apply the mooring designs and cable sizes within a layout optimization to create layouts of the wind turbines, the mooring lines, and the power cables that minimize LCOE considering the spatial dependencies from wind rose data, lease area boundaries, and required array cables. After the layout is optimized, we implement the 3D dynamic cable designs and adjust the chosen layout's cable routing algorithmically with limited manual adjustments to prevent clashes between the cables and moorings or anchors. This completes the reference floating wind array design for each region.

To serve as general reference designs, each site's characteristics are simplified to use a uniform seabed and square lease area, and the export cable to shore is not included.

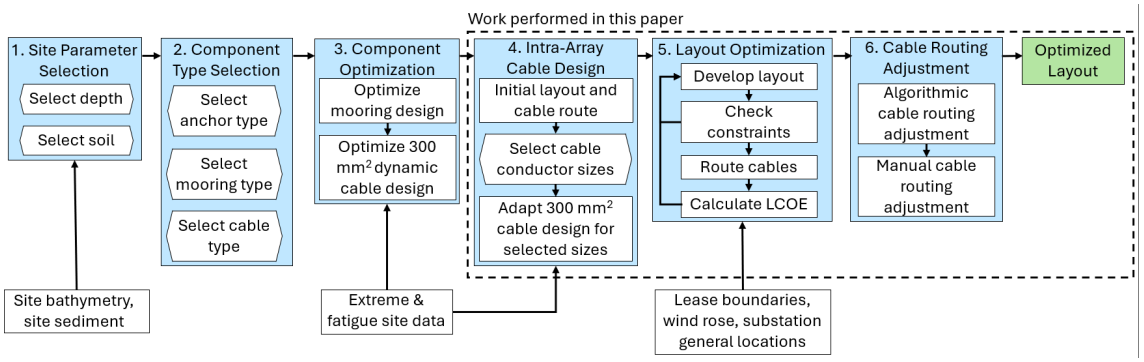

Figure 1. Array design process overview.

2.1 Site parameter selection

We considered representative site-specific seabed and metocean conditions when developing the reference array designs. These inputs are based on reference site conditions defined by Biglu et al. (2024b), which combine metocean data for each site from several sources – including the National Data Buoy Center, NLR's National Offshore Wind Dataset, and the High Frequency Radar Network – and include extrapolated extreme metocean parameters at different return periods and a set of "fatigue bins" that represent the joint probability distribution of the site's wind and wave conditions. The methodology used to develop the datasets in Biglu et al. (2024b) is described in Biglu et al. (2024a). As detailed in Sect. 2.2.3, the mooring systems were designed for both ultimate and fatigue loads, relying on the processed extreme and fatigue metocean data from Biglu et al. (2024a). The dynamic power cables were designed for extreme loads.

In the present work, we developed wind roses for each site from the same site condition dataset (Biglu et al., 2024b) for use during the array layout optimization process. We also used the extreme metocean data in load cases to check dynamic power cable designs and the floating substation designs. By adhering to the existing well-defined reference site conditions, additional research on the reference designs can look more deeply into various load cases of interest.

The reference array designs are meant to be representative of the general regions they were designed for rather than fitting in a specific lease area; therefore, we assume that all lease areas have a constant depth and soil type representative of the region and that the area boundaries are square. The representative depth and soil type are based on the bathymetry and soil data found in Biglu et al. (2024b). The size of each area is loosely based on the size of the lease areas in each region.

2.2 Subsystem and component design

The reference arrays use reference component and subsystem designs developed in previous work when available and relevant to the needs of each site. The following subsections detail the design selections and the nature of any design adaptations.

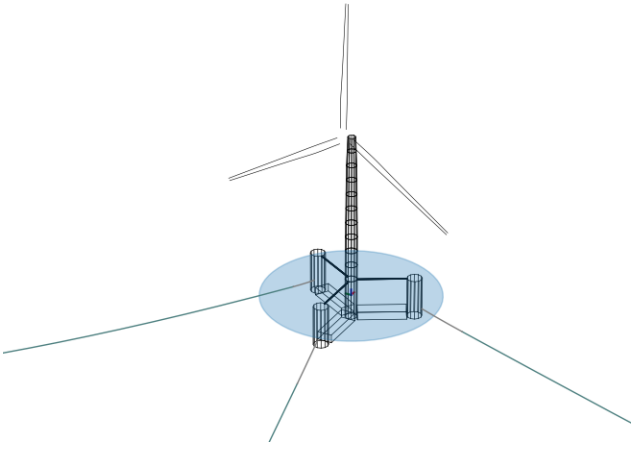

Figure 2. RAFT model of VolturnUS-S semisubmersible and IEA Wind 15 MW wind turbine.

2.2.1 Floating wind turbine

The floating wind turbine assumed for the reference array designs is the IEA Wind 15 MW reference turbine (Gaertner et al., 2020). It is a widely used reference wind turbine design, developed through a collaborative effort as part of the IEA Wind Task 37 on Wind Energy Systems Engineering. The platform is the University of Maine VolturnUS-S reference semisubmersible (Allen et al., 2020), which was specifically designed for the IEA Wind 15 MW turbine. The VolturnUS-S is a generic steel semisubmersible with three radial columns and a central column that holds the tower. The platform and wind turbine are shown in Fig. 2, and their properties are summarized in Table 1. The VolturnUS-S platform with the IEA Wind 15 MW turbine provides a well-established floating wind turbine system for the reference array designs.

Table 1. VolturnUS-S and IEA 15 MW reference wind turbine properties.

Parameter	Value
Turbine rating (MW)	15
Hub height (m)	150
Rotor diameter (m)	240
Rated wind speed ($m\,s^{-1}$)	10.59
Freeboard (m)	15
Draft (m)	20
Platform mass (t)	17 839
Tower mass (t)	1263
RNA mass (t)	991
Hull displacement (m^3)	20 206

Table 2. Floating offshore substation design developed by Jorge Alcantara (2023).

Parameter	Value
Platform length (m)	54.78
Platform width (m)	54.78
Cable deck height above mean water level (m)	12.00
Draft (m)	22.00
Mass (mT)	29 084
Vertical center of gravity below mean water level (m)	5.63

The VolturnUS-S was originally designed with a chain catenary mooring system for a 200 m depth. We replaced the mooring system with designs from Lozon et al. (2025) to suit the water depths of the reference array designs. Section 2.2.3 discusses the mooring designs in more detail. We also added dynamic power cables (Sect. 2.2.5), which were not included with the original VolturnUS-S design.

2.2.2 Floating substation

The floating offshore substation design used in these arrays is a rectangular semisubmersible high-voltage alternating current (HVAC) substation developed by Jorge Alcantara (2023). This design has a capacity of 1.2 GW. The platform comprises four square columns connected in a square with four pontoons. The dimensions and mass properties of the floating substation platform are shown in Table 2. The geometry of the floating substation platform is visualized in Fig. 3.

As with the floating wind turbine, we applied the mooring line and dynamic cable designs developed in Lozon et al. (2025) to the floating substation; however the substations feature a larger number of mooring lines to ensure redundancy of the design. A substation failure would have a more significant impact on farm revenue than a single turbine failure, so a redundant mooring system is of greater importance. We verified the performance of each mooring system and substation

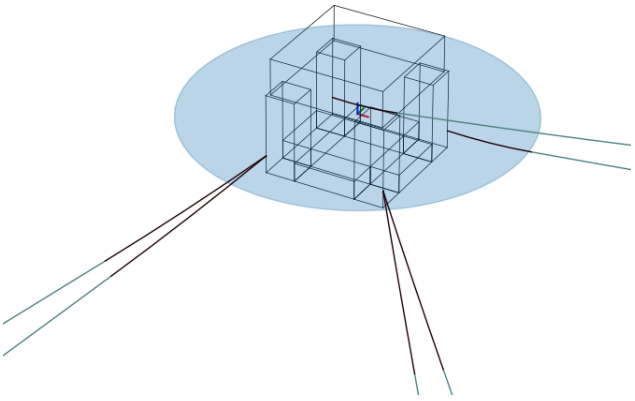

Figure 3. RAFT model of floating substation.

under a 500-year return period of extreme wind, wave, and current loading in the open-source frequency domain modeling tool RAFT (Hall et al., 2022a) to ensure acceptable platform offsets for the dynamic cable designs. The dynamic performance of the substation platform, which was designed and evaluated in Jorge Alcantara (2023), is not a focus of the present work. All substations feature intra-array cable connections on a maximum of three of the four sides; one side is free of cables to allow maintenance vessel access.

2.2.3 Mooring system

The mooring systems in the reference array designs were previously developed in Lozon et al. (2025) for the same sets of site conditions. These designs each have a different configuration (catenary, semitaut, and taut in order of increasing depth). They were optimized for the extreme and fatigue site conditions in a multifidelity modeling process consisting of (1) the optimization of line dimensions to minimize costs subject to initial constraints checked in the quasi-static mooring model MoorPy (Hall, 2024), (2) extreme and fatigue load analyses using the dynamic floating wind turbine modeling tool OpenFAST (Jonkman et al., 2023), and (3) adjusting tuning factors in the quasi-static optimization and iterating until all constraints were satisfied. The design constraints included maximum tensions, fatigue life of chain sections, avoiding polyester rope contact with the seabed, yaw stability, avoiding vertical loading on drag-embedment anchors, and platform offset. The extreme load analysis applied aligned wind and wave directions to obtain peak loading on the mooring system, while the fatigue load cases considered site-specific wind–wave misalignment. The fatigue and extreme load cases are provided in Biglu et al. (2024b), and the methodology used to develop these datasets is described in Biglu et al. (2024a). This design process and the resulting designs are detailed further in Lozon et al. (2025).

We used these mooring system designs directly for the floating wind turbines in the reference array designs, relying on the extreme and fatigue load analyses and constraint

checks that were performed in Lozon et al. (2025); however, for the floating substations, we used the same mooring line designs but increased the number of mooring lines to six or eight to provide increased restoring stiffness and redundancy. We verified that the substation mooring systems keep the platform offsets within acceptable limits under extreme current loading.

2.2.4 Anchors

Detailed anchor design was not a focus of this work, but anchor costs significantly contribute to the overall array cost; therefore, approximate anchor masses were directly pulled from Lozon et al. (2025), which sized anchors based on maximum anchor loads from extreme load cases performed in OpenFAST and general soil types. We input these approximate anchor masses into our anchor cost modeling assumptions described in Sect. 2.3.3 to estimate the anchor material costs.

2.2.5 Power cables

The reference array designs include intra-array cables between the turbines and from the turbines to the substation. Each intra-array cable connecting two floating wind turbines or a floating wind turbine and a substation consists of a dynamic cable on either end to connect to the platform and a static cable routed along the seabed between the dynamic cables.

The dynamic cable designs were developed in Lozon et al. (2025) following a similar design process to the moorings. That work initially optimized the cable dimensions and checked constraints in MoorPy, and then it checked the dynamic cables in OpenFAST against constraints for extreme tensions and allowable curvature in extreme load cases, iterating until all constraints were met. More details on the design process of the dynamic cables can be found in Lozon et al. (2025).

For the gigawatt-scale reference floating wind farms, additional dynamic cable designs were needed for larger conductor sizes. These larger conductor sizes are necessary to meet the power transmission needs when many turbines are connected in series within the wind farm. We adapted the dimensions of the initial designs from Lozon et al. (2025), which use a cable with a 300 mm^2 conductor cross-sectional area, for larger conductor sizes (630 and 1000 mm^2) by increasing the number of buoyancy modules to compensate for the increased cable weight. This approach maintains approximately the same cable profile shapes and ranges of motion. We then simulated these additional cable designs in conjunction with the floating wind turbine and mooring system for extreme load cases in OpenFAST to ensure compliance with the allowable cable tensions and curvatures. The extreme load cases featured aligned wind and waves to obtain peak loading.

The properties for each dynamic cable are shown in Table 3. For all dynamic cable designs, we assumed a buoyancy module with a volume of 0.57 m^3, consistent with the original reference designs. The buoyancy module properties are shown in Table 4.

The static cables are represented by their routing along the seabed and their cross-sectional properties. Cable burial and environmental loadings are beyond the reference design scope. The properties for each static cable are shown in Table 5.

2.3 Layout

To develop the reference array layouts, we used and expanded on an NLR-developed layout optimization tool described in Hall et al. (2024a) and Sirkis et al. (2025) to minimize the LCOE. This tool considers moorings, anchors, and cables, and it is capable of interfacing with a variety of optimizers. Figure 4 summarizes the array layout design process, which is described in the following subsections.

2.3.1 Layout design parameterization

Each reference array layout follows a uniform-grid approach with seven key design variables that control the grid geometry. We chose a uniform grid to maintain navigability within the array, following the United States Coast Guard recommendations (United States Department of Homeland Security and United States Coast Guard, 2024). The design variables we used for these uniform-grid layout optimizations are as follows:

- D'_x, D'_y: grid x, y spacing (m)
- x_0, y_0: grid x, y translation from centroid (m)
- α: grid rotation (°)
- β: grid skew (°)
- γ: platform rotation (°).

The grid variables are shown in Fig. 5. The platform rotation variable, γ, is defined as 0° when one platform leg (or mooring line) is due north. Platform rotation definitions are independent of the grid rotation angle α. All angles are measured clockwise positive.

The substation rotation is defined at 0° when one pontoon faces each cardinal direction. We set the substation heading after the optimization process based on the spatial requirements of the array and the direction of the incoming dynamic cable strings.

We altered the uniform-grid layout optimization methodology in Sirkis et al. (2025) to improve the computational efficiency and give more consistent results. The previous method tested each potential platform location against spatial constraints before adding that grid location to the layout,

Table 3. Dynamic cable properties.

Parameter	Cable type 1	Cable type 2	Cable type 3
Conductor size (mm^2)	300	630	1000
Outer diameter (m)	0.161	0.184	0.203
Linear density ($kg\,m^{-1}$)	36.66	55.76	75.74
Axial stiffness (MN)	469	658	854
Bending stiffness ($kN\,m^2$)	19.92	42.47	68.73
Min bearing load (kN)	383.2	537.4	698.4
Min bending radius (m)	2.41	2.76	3.05

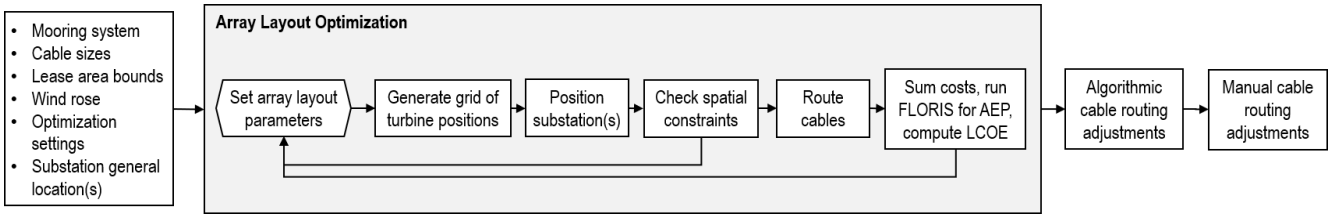

Figure 4. Array layout design process.

Table 4. Buoyancy module properties.

Parameter	Value
Displaced volume (m^3)	0.566
Mass (kg)	270.68
Overall density ($kg\,m^{-3}$)	500
Length (m)	0.90
Diameter (m)	0.865

and it stopped adding points when the required number of platforms was met. In the current method, we develop a grid of all possible platform location points inside the lease area without determining if the constraints are met. In cases where more grid points than the required number of platforms fit inside the boundary, points closest to the boundary are removed until the required number of platforms remain. This ensures that the array layout is approximately centered within the lease area.

Platforms closest to the boundary are generally most at risk of violating spatial constraints, such as mooring system components crossing the boundary; therefore, when generating the layouts, we keep the platform locations with the best chance of passing spatial constraint checks without checking the constraints of every possible grid point. Layout constraints are checked all together at a later step for the grid platforms to improve efficiency. When less than the required number of platforms fit in the boundary, the layout is excluded from consideration.

2.3.2 Substation placement and preliminary cable routing

Cable routing within the array is dependent on the location of the substation(s), and the intra-array cables are an important contributor to cost; therefore, it is important to accurately represent the substation placement during the layout optimization.

To maintain navigability of the array, we assume that substations must be positioned on the same uniform grid as the turbines. The approach in Sirkis et al. (2025) kept the substation location constant during the optimization process, which does not allow the substation location to be part of the grid. Our current approach places substations in the uniform grid at the grid points closest to the user-inputted substation positions. This allows the user to choose the general substation locations while ensuring that the substations fit within the layout's uniform grid. The total number of grid points maintained when developing the platform locations, as described in Sect. 2.3.1, includes the total number of turbines plus the number of substations to accommodate substations in the grid.

Once the substation positions are defined, an approximate cable routing is automatically performed within the optimization loop. This cable routing allows for an approximation of the cable costs during the optimization. We then refine the cable routing after the optimization is finished, as discussed in Sect. 2.3.6.

When there are multiple substations in the array, we first assign each turbine to a substation before determining the cable routing. This differs from Sirkis et al. (2025), which only supported one substation. To support multiple substations, we use an assignment algorithm that allocates turbines

Table 5. Static cable properties.

Parameter	Cable type 1	Cable type 2	Cable type 3
Conductor size (mm^2)	300	630	1000
Outer diameter (m)	0.154	0.177	0.197
Linear density ($kg\,m^{-1}$)	30.18	45.33	60.87
Axial stiffness (MN)	287	417	551
Bending stiffness ($kN\,m^2$)	7.68	17.60	29.59
Min bearing load (kN)	183.7	260.5	342.8
Min bending radius (m)	2.31	2.66	2.95

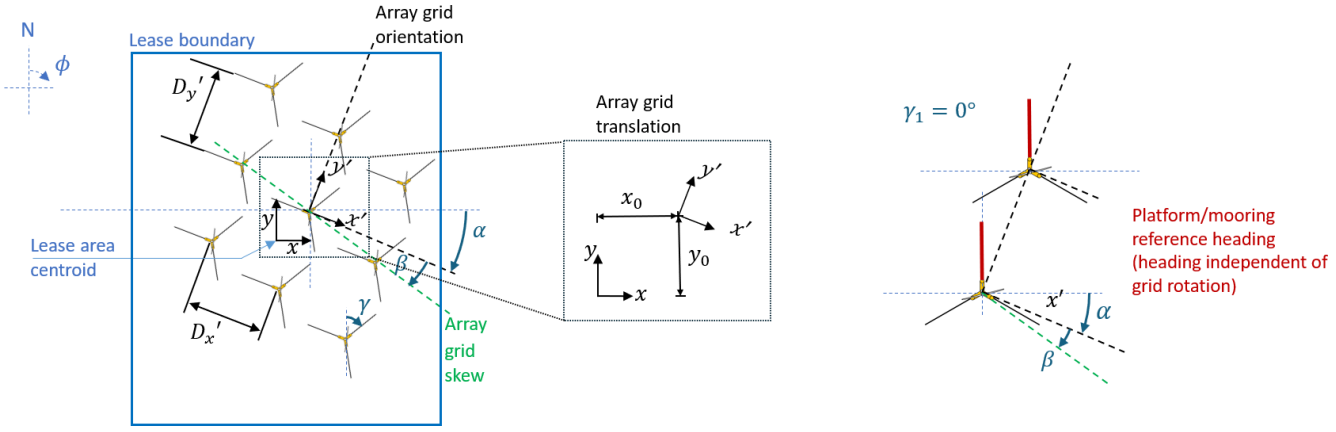

Figure 5. Grid design variables, adapted from Hall et al. (2024b).

to their closest substation to reduce cable costs. If the number of turbines connected to a substation exceeds the substation's capacity, turbines that have the smallest difference in distance to an alternate substation from the overwhelmed substation are re-allocated to the alternate substation until each is at or below capacity.

After each turbine is assigned to a substation, we apply the cable routing approach described in Sirkis et al. (2025) for the pool of turbines assigned to each substation. First, the clusters of turbines to be connected in series are determined using spectral clustering around the substation. Then, the routing within the clusters is determined using Prim's algorithm (Prim, 1957), a minimum spanning tree method. Sirkis et al. (2025) describe this intra-array cable routing algorithm in detail. The conductor size for each cable is determined based on the power requirements from the number of upstream turbines, which affects the cost, as described in Sect. 2.3.3.

2.3.3 Optimization objective function

The objective of the layout optimizations is to minimize the LCOE. To improve computational efficiency, the optimization framework only calculates the LCOE for layouts that meet all constraints described in Sect. 2.3.4. The LCOE can be described as

$$\mathrm{LCOE} = \frac{\mathrm{FCR} \times \mathrm{CapEx} + \mathrm{OpEx}}{\mathrm{AEP}}, \tag{1}$$

where FCR is the fixed charge rate, defined as the fraction of capital expenditure (CapEx) that will be paid each year; CapEx is the total capital expenditure for the array, including the installation and component costs; OpEx is the annual operational expenditure; and AEP is the annual energy production.

The array AEP is calculated using the Gaussian curl hybrid wake model within the steady-state wake modeling tool FLORIS (v4.2) (Gebraad et al., 2014). The wind roses we used in the AEP calculations cover each direction at intervals of 5° for every wind speed at intervals of $1\,m\,s^{-1}$.

For the layout optimization, all CapEx costs except for those of the intra-array cables are assumed constant throughout the optimization. The intra-array cable material costs are updated for each feasible layout considered in the optimization based on the output cable routing. During the optimization, these cable costs are approximated by the two-dimensional distance between turbines multiplied by the dynamic cable cost per meter. This simplification is used to improve computational efficiency. It results in shorter cable lengths than a three-dimensional representation; however, the cost reduction is partially offset by the higher dynamic cable

cost in comparison with static cables. The cable cost per unit length for a 66 kV dynamic cable is modeled as

$$\text{Cost}_{\text{iac}} = (0.7845\,\text{USD}\,\text{mm}^{-2}\,\text{m}^{-1})A + 257.3\,\text{USD}\,\text{m}^{-1}, \quad (2)$$

where Cost_{iac} is the dynamic intra-array cable cost per unit length, and A is the cable conductor area. The dynamic cable cost values are based on a linear regression of the costs provided in Hall et al. (2024b).

The mooring material cost is calculated as follows:

$$\text{Cost}_{\text{chain}} = (2.585\,\text{USD}\,\text{kg}^{-1}\,\text{m}^{-1})m, \quad (3)$$

$$\text{Cost}_{\text{poly}} = (23\,\text{USD}\,\text{MN}^{-1}\,\text{m}^{-1})\text{MBL}, \quad (4)$$

where $\text{Cost}_{\text{chain}}$ is the mooring chain cost per unit length, m is the linear mass density of the chain, $\text{Cost}_{\text{poly}}$ is the mooring polyester cost per unit length, and MBL is the minimum breaking load of the polyester. The chain cost coefficient is based on the value provided in Hall et al. (2022b), and the polyester cost coefficient is based on industry-provided estimates.

The anchor material costs are determined based on the material cost per kilogram as follows:

$$\text{Cost}_{\text{DEA}} = (5.705\,\text{USD}\,\text{kg}^{-1})m, \quad (5)$$

$$\text{Cost}_{\text{SPA}} = (4.435\,\text{USD}\,\text{kg}^{-1})m, \quad (6)$$

where Cost_{DEA} is the material cost of the drag-embedment anchors, Cost_{SPA} is the material cost of the suction pile anchors, and m is the anchor mass. These material cost coefficients are based on the average cost per mass value provided in Hall et al. (2024b). Because of the constant bathymetry in the arrays, one mooring and anchor design is used for all platforms in a given array, so the mooring and anchor cost remains constant for each array optimization.

The remaining CapEx costs and the OpEx costs are based on the data and assumptions provided in Housner and Mulas Hernando (2024). The CapEx costs excluding mooring, cable, and anchor materials are calculated at a rate of 3749 USD kW^{-1} of capacity. Annual OpEx costs are calculated at a rate of 62.5 USD kW^{-1} of capacity. The FCR is set at 5.82 %.

After the optimization, we implement realistic three-dimensional cable designs with lazy-wave cable configurations at each platform connected to static cable sections along the seabed, as described in Sect. 2.2.5. Additionally, we refine the cable routing around the substation and to avoid moorings and anchors, which is described in Sect. 2.3.6. The additional component cost calculations used in the three-dimensional representation of the cables are described in the following.

Buoyancy module costs are calculated as

$$\text{Cost}_{\text{buoy}} = (8590\,\text{USD}\,\text{m}^{-3})\,V + \text{USD}\,3080, \quad (7)$$

where $\text{Cost}_{\text{buoy}}$ is the buoyancy module cost, and V is the buoyancy module volume. These values were determined from industry estimates.

Static cable costs are calculated as

$$\text{Cost}_{\text{static}} = (0.719\,\text{USD}\,\text{mm}^{-2}\,\text{m}^{-1})\,A + 239.57\,\text{USD}\,\text{m}^{-1}, \quad (8)$$

where $\text{Cost}_{\text{static}}$ is the cost per unit length, and A is the cable conductor area.

The estimated costs of the cable connectors, which include bend stiffeners, are as follows for each cable:

$$\text{Cost}_{\text{connectors}} = (212.22\,\text{USD}\,\text{mm}^{-2})\,A + \text{USD}\,139\,831, \quad (9)$$

where $\text{Cost}_{\text{connectors}}$ is the cable connector cost per cable.

Cable joints, found at the transition between the dynamic and static cable sections, are modeled as a constant cost of 237×10^3 per turbine. The static cable, cable connectors, and cable joint costs are based on the data provided in Hall et al. (2024b). The static cable and cable connector costs are a linear regression of the data provided in Hall et al. (2024b).

We have collected cost data from various sources to compare the assumed component costs with values from a limited literature search. The limited number of publicly available cost estimates for different components is a challenge when comparing cost estimates, as is the wide range of costs reported for certain component types. Table 6 summarizes costs gathered from the literature compared to the cost values used in this work. Where possible, we have attempted to use data sources that allow for fair comparisons between components, and converted costs to 2024 US dollars (USD). In the process of developing these cost comparisons, we have included some assumptions to allow for consistent cost comparisons when the only component costs available were reported using different units of measure than those used in the present work. The discussion following the table provides more details on these assumptions.

Dynamic cable cost data are particularly challenging to find, especially cost data that vary with conductor size. A 2007 study (Green et al., 2007), which gathered cable costs from two companies, reported intra-array cable cost ranges for a variety of conductor sizes. The cost values reported in Table 6 from Green et al. (2007) have been adjusted for inflation from 2007 USD to 2024 USD. Note that this literature source does not differentiate between static and dynamic cable costs, so the same values are applied to the static and dynamic cables for the purposes of comparison. The cost values from Green et al. (2007) are higher than the utilized cost in general. Significant supply chain development and innovation in the offshore intra-array cable industry since 2007 may have led to reduced costs.

Buoyancy modules are another component with limited cost data available. Hall et al. (2024b) provide buoyancy module costs per cable for an array of conductor sizes. To compare costs with those used in this work, we assumed the cable (which has two dynamic cable sections, one to connect to each platform) has the same volume of buoyancy modules as the dynamic cable designs used in this work. We es-

Table 6. Component cost comparison between utilized values and values from the literature.

Component	Unit	Utilized cost	Utilized source	Costs from literature	Literature source
Dynamic cable 300 mm^2	USD m^{-1}	493	Hall et al. (2024b)	486–847	Green et al. (2007)
Dynamic cable 630 mm^2	USD m^{-1}	752	Hall et al. (2024b)	821–1033	Green et al. (2007)
Dynamic cable 1000 mm^2	USD m^{-1}	1042	Hall et al. (2024b)	1196–1240	Green et al. (2007)
Static cable 300 mm^2	USD m^{-1}	455	Hall et al. (2024b)	486–847	Green et al. (2007)
Static cable 630 mm^2	USD m^{-1}	693	Hall et al. (2024b)	821–1033	Green et al. (2007)
Static cable 1000 mm^2	USD m^{-1}	959	Hall et al. (2024b)	1196–1240	Green et al. (2007)
Buoyancy modules	USD m^{-3}	11 670	Industry estimate	12 560–14 035	Hall et al. (2024b)
Cable connectors 300 mm^2	USD per cable	203 500	Hall et al. (2024b)	NA	NA
Cable connectors 630 mm^2	USD per cable	273 500	Hall et al. (2024b)	NA	NA
Cable connectors 1000 mm^2	USD per cable	352 000	Hall et al. (2024b)	NA	NA
Cable joints	USD per turbine	237 000	Hall et al. (2024b)	NA	NA
Suction pile anchor	USD kg^{-1} mass	4.435	Hall et al. (2024b)	4.11	van Koten (2021)
Drag-embedment anchor	USD kg^{-1} mass	5.705	Hall et al. (2024b)	4.15	Davies et al. (2025)
				5.30	Quoceant (2016)
Chain	USD kg^{-1} mass	2.585	Hall et al. (2022b)	2.54–6.34	Hall et al. (2024b)
				4.28	Davies et al. (2025)
				1.68	Quoceant (2016)
Polyester	USD MN^{-1} m^{-1}	23	Industry estimate	16.5	Hall et al. (2024b),
				43	Davies et al. (2025)

NA – not available.

timated the cost per volume of buoyancy module from the cable buoyancy module cost divided by the total buoyancy module volume for each dynamic cable size. The range of buoyancy module costs is based on the minimum and maximum values from the three cable sizes used in this work. The buoyancy module costs estimated from Hall et al. (2024b) are somewhat higher than the values used in this work, but it is difficult to directly compare them due to the required assumptions.

Relevant cost data for cable connectors and joints, especially for conductor sizes similar to those used in this work, were not found in the limited literature review. Quoceant (2016) provided costs for static and dynamic bend stiffeners, which convert to approximately USD 120 000 in 2024 USD for all required bend stiffeners in one cable. However, this cost is not comparable to the value used in this work because it is for a different cable conductor size and does not include costs of other cable connection parts. It is therefore not included in Table 6.

van Koten (2021) provided a cost estimate of suction pile anchors, which was obtained from an industry estimate. We converted the value to USD using 2021 exchange rates and adjusted for inflation from 2021 to 2024 USD. Van Koten's reported cost coefficient is similar to the value used in this work.

Two cost sources were found for drag-embedment anchors in addition to the source used in this work. Hall et al. (2024b) provided a range of drag-embedment anchor cost coefficients, and the average value was used in this work. Davies et al. (2025) reported a lower cost coefficient, while a report from Wind Energy Scotland (Quoceant, 2016) provided an approximate cost coefficient closer to the utilized value after converting to 2016 USD and adjusting for inflation to 2024 USD.

Three chain cost per mass coefficients are reported in Table 6 in addition to the value used in this work. Hall et al. (2024b) reported a cost range of 2.54–6.34 USD kg^{-1}, and Davies et al. (2025) reported a cost coefficient near the center of this range. Quoceant (2016) provided a lower estimate at 1.68. The value used in this work, 2.585, is within the range of other reported values.

The polyester cost coefficient used in this work is in between the cost coefficient values provided in Hall et al. (2024b) and Davies et al. (2025).

2.3.4 Spatial constraints

Spatial constraints are checked during the array layout optimization to ensure realistic and feasible designs. The spatial constraints apply buffer zones around the mooring lines, anchors, and platforms to ensure that these components do not cross each other and stay within the boundaries of the lease. Figure 6 shows the buffer zones that are applied around a single floating wind turbine.

We use the same approach to buffer zones as laid out in Hall et al. (2024a). Anchor buffer zones have a 100 m diameter centered around the anchor, which ensures that no two anchors are less than 100 m apart, per ISO (2005). The mooring buffer zones have a 40 m diameter centered along the axis

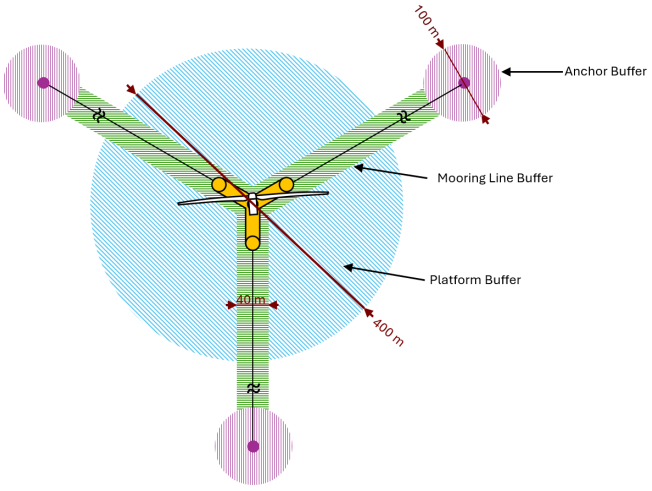

Figure 6. Anchor, mooring, and platform buffer zones (top-down view).

of the mooring line. Mooring buffer zones may not cross anchor buffer zones or other mooring buffer zones, and anchor buffer zones may not cross other anchor buffer zones. Platforms also have a buffer zone with a 400 m diameter. The spacing between turbines is set to a lower limit of 0.6 nautical miles or 1111 m, but the platform buffer zone ensures a minimum distance from the lease boundary edge. Mooring line and anchor buffer zones may cross the platform buffer zone. To keep the design within the lease area boundaries, no buffer areas are permitted to cross a boundary.

We do not check if cables cross mooring lines or other components in the optimization process because the cable routing developed in the optimization is designed to estimate cable costs by simply determining the shortest distance between connected platforms rather than determining the exact route of a cable between two platforms; therefore, cables do not have buffer zones within the optimization. This simplification is used to improve the computational efficiency of the optimization. After the optimization is completed, a full three-dimensional representation of the cables is implemented. The dynamic cable headings and the static cable routing points are then adjusted to avoid mooring and anchor clashing, as described in Sect. 2.3.6. As discussed in Sect. 2.3.3, the cost difference is limited and does not greatly affect the total.

2.3.5 Optimization approach

The layout optimization, where the grid parameters are adjusted to minimize the LCOE while meeting spatial constraints, can be done with many types of optimizers. We chose a particle swarm optimizer for its ability to find the global minimum even when there are discontinuities and many local minima. A particle swarm optimizer is a gradient-free optimization method developed by Kennedy and Eberhart (1995), based on the natural phenomenon of animals' collective behavior in a swarm, such as schooling fish. An initial randomized group (swarm) of particles, each representing a potential solution in the design space, is evaluated, and each particle moves within the design space at each iteration. Each particle considers its best known solution and the swarm's best known solution at the end of each iteration when new particle positions are generated. If a particle's position fails any constraints, the particle's best position will not be updated, and the particle is not considered when updating the overall swarm's best position at the end of the iteration. Therefore, the optimizer does not allow the solutions of non-feasible positions to influence the future velocity of the particle or swarm. This method requires many function evaluations per iteration, but it allows the optimizer to move past local minima.

For this work, we used a swarm size of 200 evaluated for a minimum of 100 iterations. The Gulf of Maine and Gulf of America optimizations were run for 100 iterations, while the Humboldt Bay optimization was run for 364 iterations due to the increased complexity of the layout, which increased the required number of iterations to achieve a general convergence.

The evolution of the particle positions and best solution were monitored throughout the optimizations. In the case of the Gulf of Maine and Gulf of America optimizations, the optimization was consistently unable to find better solutions well before 100 iterations, and the swarm's particle positions were concentrated around the swarm's best known solution, so only 100 iterations were used for those designs. In the case of the Humboldt Bay optimization, new best solutions were frequently being discovered by the optimization at around the 100 iteration mark, so the optimization run time and number of iterations were increased until new iterations were consistently unable to determine a better solution.

Note that the goal of this work is to develop and present detailed, open-source array layout designs that approximately minimize the LCOE while meeting the constraints and design requirements of each region; therefore, a detailed study of the optimization algorithms, settings, and convergence criteria that lead to the global minimum LCOE is out of scope.

2.3.6 Post-optimization cable routing and adjustment

After the layout optimization is completed, we refine the preliminary intra-array cable routing with an algorithmic approach that identifies and adjusts cables that are at risk of clashing with mooring lines. We apply an angular buffer on all mooring lines along the mooring line heading, and we examine if a dynamic cable heading lies within the angular buffer zones of the platform it is attached to. A 30° angle is used by default, but we adjust this value to fit the unique spatial requirements of each array. The angular buffer begins at the center of the platform and extends for 500 m past the cable attachment point on the platform. Cables that cross the

buffer are adjusted to follow the outside of the angular buffer for 500 m from the cable attachment point or for the horizontal span of the dynamic cable, whichever is longer.

After this distance, cables begin routing toward the next turbine, even if the mooring radius is larger than 500 m, because the angular buffer increases the distance from the mooring with length. Continuing the angular buffer for the entirety of the mooring line length could cause the cable to interfere with the moorings of other turbines for locations with large mooring footprints, such as Humboldt Bay. Figure 7 shows this process.

If a static cable overlaps with an anchor buffer zone, we reroute the cable around the anchor with an additional routing point placed 100 m from the anchor point in a direction perpendicular to the initial cable heading, as shown in Fig. 8.

We also apply some manual routing adjustments to cables at the substation. Cables attaching to a substation are rerouted to ensure that one side of the substation is clear of cables and to avoid acute angles when possible for the static cable routing. The headings of the dynamic cables entering the substation are spaced at 5° intervals to prevent clashing between dynamic cables.

3 Reference array designs

We developed reference array designs for reference site conditions representative of three regions: Humboldt Bay, the Gulf of Maine, and the Gulf of America. Each region distinctly varies in water depth and metocean conditions. Following the methodology outlined in Sect. 2, we applied the mooring system and dynamic cable designs and developed optimized array layouts and cable routing for each region.

The Humboldt Bay and Gulf of America reference arrays feature 67 turbines for approximately 1 GW of installed capacity, while the Gulf of Maine reference array features 132 turbines for approximately 2 GW of installed capacity. The Gulf of Maine array is larger to match the capacities of the proposed lease areas in that region.

A summary of the design characteristics for each region is shown in Table 7.

The following subsections further describe each reference array design.

3.1 Humboldt Bay

The Humboldt Bay array design uses taut mooring systems, which are suitable for the deep-water depth of 800 m, and lazy-wave dynamic cables. The array consists of 67 turbines, resulting in a capacity of 1.005 GW. There is a single substation, located near the center of the array, with nine cable strings. We chose a central location prior to the optimization to reduce the required length of the large-conductor-size intra-array cables. The optimizer then placed the substation at the grid point closest to the center of the array. The array design was challenged by large anchoring radii for the mooring systems and long dynamic cable spans, which required more careful positioning of elements within the full wind farm to maintain the necessary clearances.

3.1.1 Site conditions

Humboldt Bay is located off the coast of California. The water depths in the Humboldt Bay lease areas range from 550 to 1100 m (Cooperman et al., 2022), with a uniform 800 m reference depth assumed for the array design. We selected a square lease area of 256 km^2 based on the size of the Humboldt Bay northeast lease area.

The Humboldt Bay area has large extreme current speeds, ranging from 0.92 to 1.44 $m\,s^{-1}$. The wind rose is mostly unidirectional, with the wind coming predominantly from the north. The wind, wave, and current roses for the Humboldt Bay reference site conditions are shown in Fig. 9. The extreme load case conditions, including the design load cases (DLCs) 1.6 and 6.1 and a survival load case (SLC), are shown in Table 8.

3.1.2 Mooring and cable design

The Humboldt Bay mooring design, developed in Lozon et al. (2025), is taut with suction pile anchors. In this work, we assume lazy-wave cables throughout the array. Figure 10 shows the Humboldt Bay mooring and dynamic cable configuration.

The Humboldt Bay mooring design is taut, consisting mostly of polyester rope with chain sections at the anchor and fairlead connections. The anchoring radius of the mooring system is 1400 m, which is significantly larger than the Gulf of Maine and Gulf of America designs. The mooring design is summarized in Table 9. Further details on the Humboldt mooring design performance can be found in Lozon et al. (2025).

The Humboldt Bay dynamic cable configuration is a lazy wave. The initial dynamic cable design for a 300 mm^2 cable was optimized by Lozon et al. (2025) with a cable span of 800 m (the horizontal distance between the platform connection and the joint or transition point to the static cable) and a buoyancy section length of 400 m. When evaluating the cable routing within the full array, we found that the large cable span made it difficult to fit mooring lines and cables without crossing. To address this, we decreased the cable span from 800 to 500 m while keeping the other cable dimensions the same. This effectively reduced the length of the dynamic cable that is always lying on the seabed. The dynamic cable designs for the 630 and 1000 mm^2 conductor areas have the same span, total cable length, buoyancy section length, and buoyancy section midpoint location; however, we optimized the number of buoyancy modules, and consequently the buoyancy module spacing, for each design. The 300, 630, and 1000 mm^2 designs require 34, 50, and 74 buoyancy modules, respectively. The buoyancy module spacing ranges from

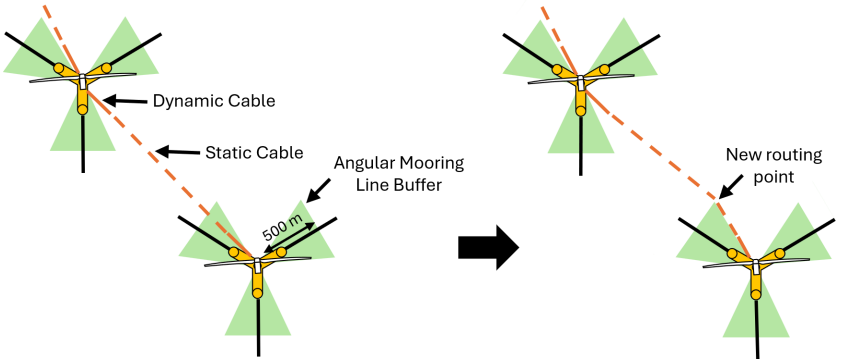

Figure 7. Cables reroute to avoid angular mooring buffers (not to scale).

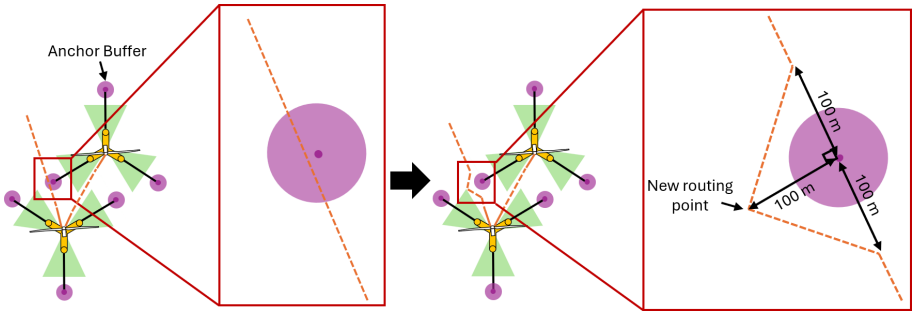

Figure 8. Cables reroute around anchor buffer zones (not to scale).

12.1 to 5.5 m. The three dynamic cable designs are summarized in Table 10.

3.1.3 Optimized layout

We optimized the Humboldt Bay array layout to maximize the LCOE. The parameters of the optimized array design are listed in Table 11. The x and y spacings are 1847.2 and 1431.3 m, respectively, and there is a small amount of skew. The grid is rotated 36.7°, maximizing spacing in the predominant wind direction of due north. The substation is located in the center of the array.

The Humboldt Bay mooring system has a large anchoring radius of 1400 m, which required careful positioning of the mooring systems to fit 67 turbines within the area. As a result, the turbine rows alternate between two opposite mooring orientations to fit the turbines more closely together. To avoid interference with mooring lines that run along the columns, we used an angular buffer of 30° to reroute the lazy-wave cables away from the mooring line heading, as described in Sect. 2.3.6. In some locations, the static cable is routed beneath the mooring lines. This maintains acceptable clearances because the taut mooring system is mostly suspended. The array layout and cable routing are shown in Fig. 11. The static cables were automatically rerouted to avoid intersecting with anchors, as shown in Fig. 12. The rerouting follows the logic outlined in Fig. 8.

The Humboldt Bay substation design features six mooring lines, with two corners supported by two mooring lines and the opposite corners supported by one mooring line each. Though it would be preferable to have two mooring lines on each corner for improved symmetry, we implemented a six-line design for Humboldt Bay due to spatial constraints. This mooring design adheres to the maximum allowable offsets dictated by the dynamic cable designs when modeled under extreme current loading. To provide sufficient clearances around this mooring system, we rerouted the dynamic cables to two sides of the substation with headings 5° apart, as shown in Fig. 13.

We designed the Humboldt Bay array layout to avoid the predominant wind direction of north–south, as shown by the wake plot in Fig. 14a. Figure 14b shows the wake losses for the array with a 12 m s^{-1} wind speed for every wind heading at 1° intervals. The wake losses are at a maximum of approximately 30 % when the wind is oriented along the columns (i.e., northwest to southeast). The wake losses are slightly less along the rows because the spacing is larger. The wind rose shows that the wind is predominantly coming from the north to northwest directions, which have minimal wake losses. This shows that the Humboldt Bay array layout was well designed to minimize wake effects.

To understand how different wind rose discretizations affect the AEP calculations, we investigated the sensitivity of the number of wind directions to the output AEP for the

Table 7. Summary of design characteristics for each region.

Parameter	Humboldt Bay	Gulf of Maine	Gulf of America
Number of turbines	67	132	67
Array capacity (MW)	1005	1980	1005
Total lease area (km^2)	256	504.5	280
Number of substations	1	2	1
Water depth	800	200	80
Mooring type	Taut	Semitaut	Catenary
Cable type	Lazy wave	Lazy wave	Lazy wave
Anchor type	Suction pile	Drag embedment	Drag embedment

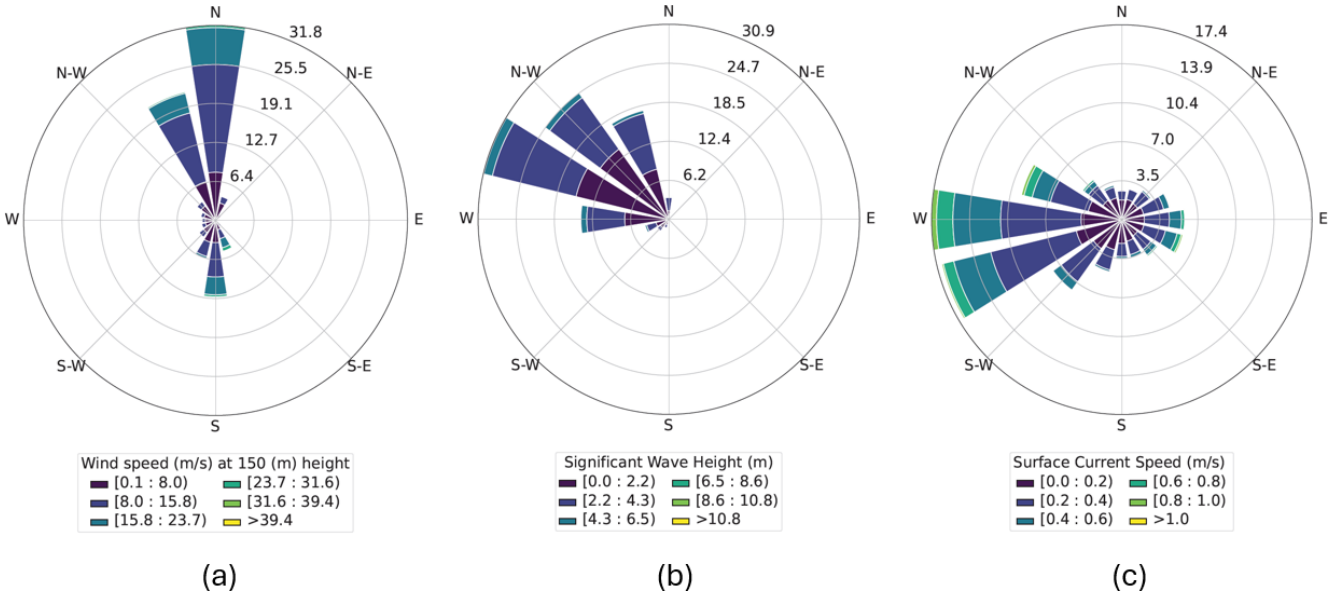

Figure 9. Humboldt Bay **(a)** wind, **(b)** wave, and **(c)** current roses (Biglu et al., 2024a).

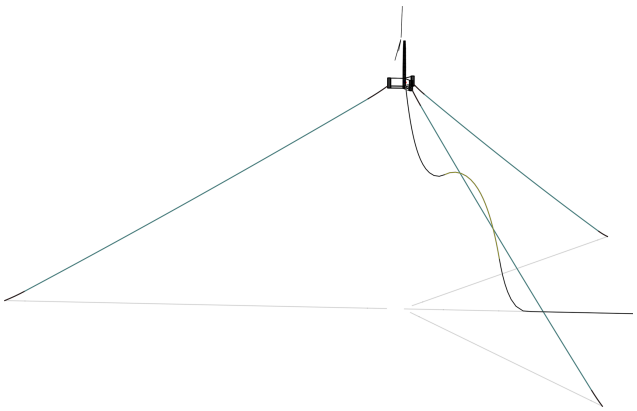

Figure 10. Humboldt Bay mooring and dynamic cable system (Lozon et al., 2025).

Table 8. Humboldt Bay extreme load case conditions.

Parameter	DLC 1.6	DLC 6.1	SLC
H_S (m)	10.5	11.8	13.7
T_P (s)	18.7	19.8	21.4
Current speed ($m\,s^{-1}$)	0.92	1.09	1.44
Wind speed ($m\,s^{-1}$)	10.59	39.44	42.97
Turbulence intensity	0.06	0.05	0.05

Humboldt Bay array. Figure 15 shows the AEP for 12, 18, 36, 72, 180, and 360 wind directions, which corresponds to intervals of 30, 20, 10, 5, 3, 2, and 1°. The highest granularity, 360 directions, produced a 0.007 TWh (0.13 %) decrease in AEP compared to the chosen granularity (72 directions, starred in Fig. 15). Lower numbers of wind directions produced more varying results, with 12 directions producing a largely underestimated AEP compared to the smallest discretization. While a wind rose discretization with 360 wind directions may produce a slightly more accurate AEP than the chosen

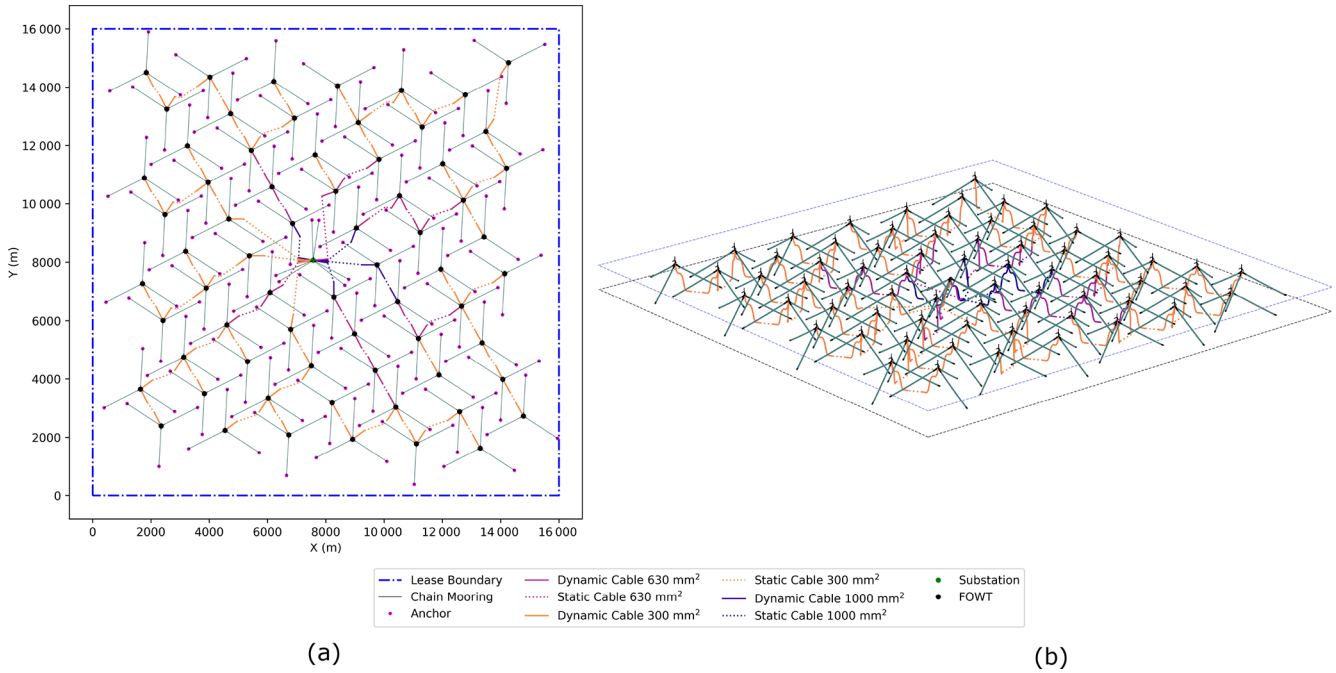

Figure 11. Humboldt Bay array layout and cable routing in **(a)** plan view and **(b)** three dimensions.

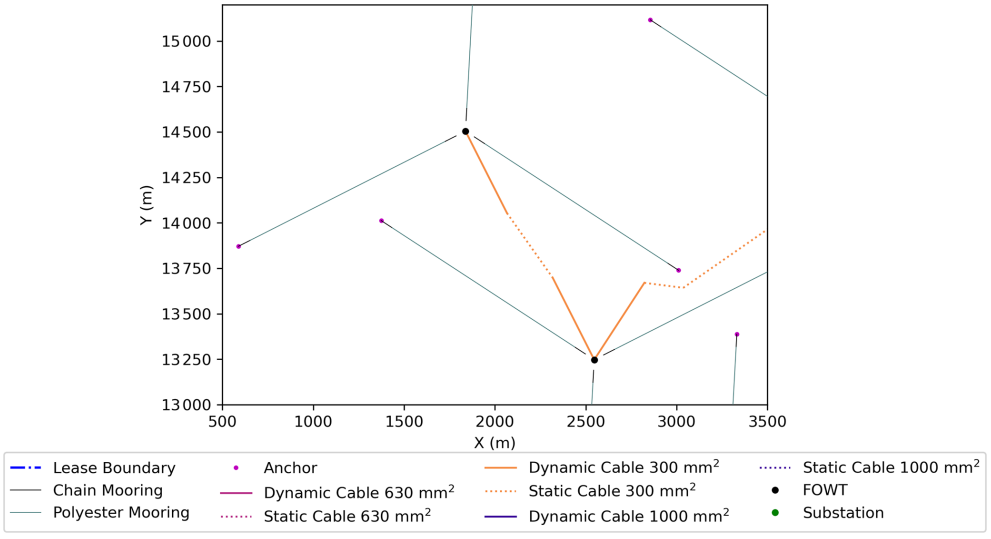

Figure 12. Humboldt Bay array cable rerouting to avoid anchors.

discretization of 72 wind directions, the chosen granularity produces a reasonably close result for significantly less computational expense.

The final values affecting the LCOE calculations in the optimization process are described in Table 12. These cost values are based on the cost curves in Sect. 2.3.3 and reflect the final design, which includes the refined cable routing. The cable material costs are significantly higher than the mooring and anchor material costs. Although there are more mooring lines than cables, the cost per length of cable is approximately 2–4.5 times that of polyester (which composes the majority of each mooring line) depending on the conductor size.

3.2 Gulf of Maine

The Gulf of Maine array design features semitaut mooring systems and lazy-wave dynamic cables. It has 132 turbines for a total capacity of 1.98 GW. Two substations are located in the array to handle the additional capacity. Each substation

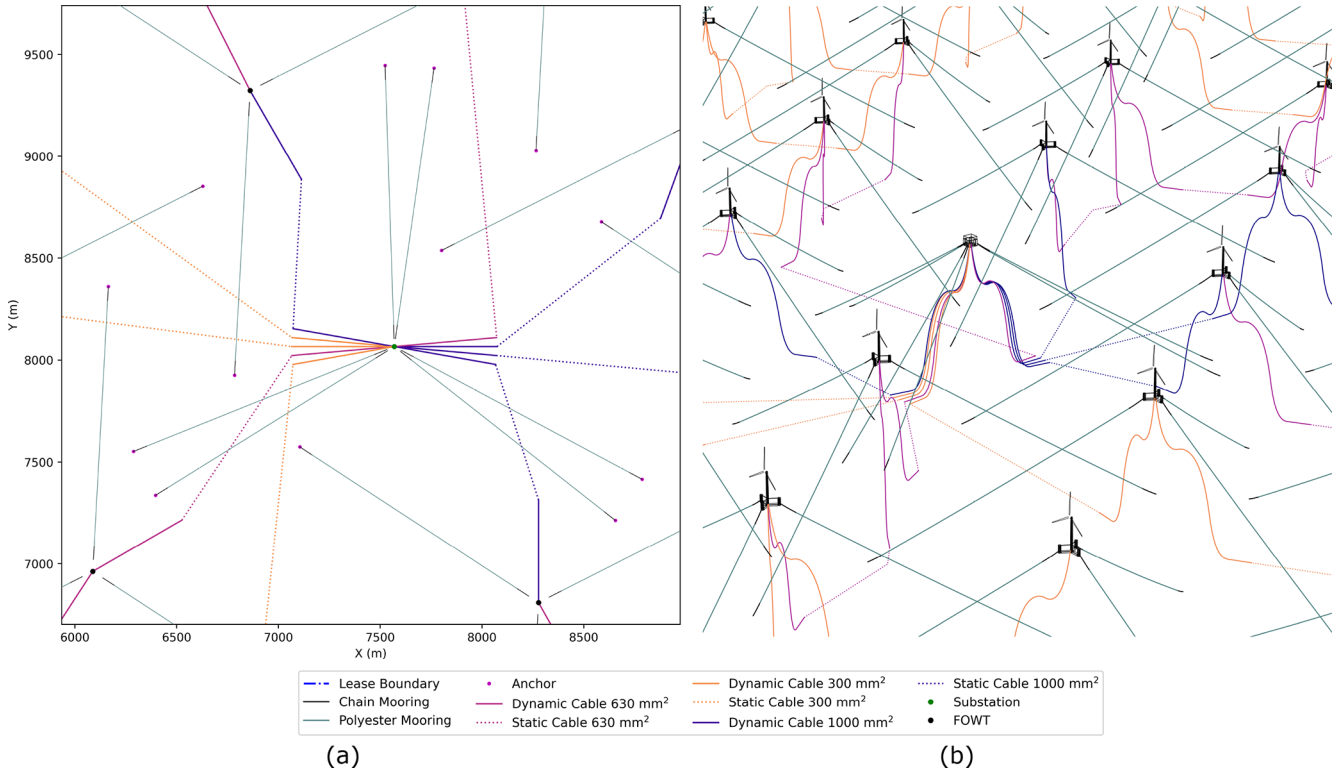

Figure 13. Final routing of intra-array cables into substation for the Humboldt Bay array in **(a)** plan view and **(b)** three dimensions.

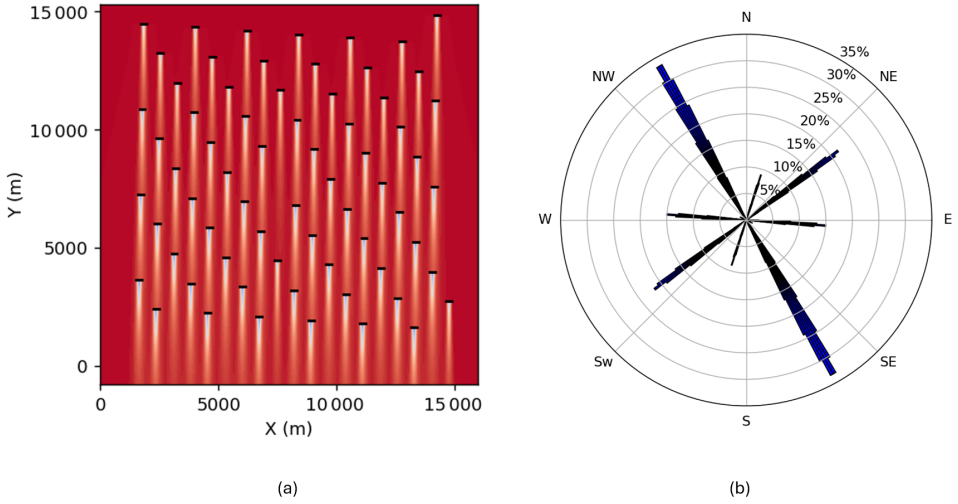

Figure 14. Humboldt Bay optimized array layout: **(a)** wakes with a wind speed of 12 m s^{-1} from due north and **(b)** percent wake losses with a wind speed of 12 m s^{-1} at each wind heading direction.

is the terminus of nine cable routes, for a total of 18 cable routes in the array.

3.2.1 Site conditions

The Gulf of Maine wind energy call area features water depths of approximately 100–300 m (Musial et al., 2023). We chose a constant water depth of 200 m for this reference array. The wind, wave, and current roses for the Gulf of Maine reference site conditions are shown in Fig. 16. The extreme load case conditions are described in Table 13.

3.2.2 Mooring and cable design

Figure 17 shows the mooring and dynamic cable configuration for the Gulf of Maine.

Table 9. Humboldt Bay mooring line design adapted from Lozon et al. (2025).

Parameter	Value
Anchoring radius (m)	1400
Fairlead radius (m)	58
Fairlead depth (m)	14
Pretension (kN)	1704
Declination angle (°)	36.6
Line section 1 material	120 mm R4 studless chain
Line section 1 length (m)	80
Line section 2 material	184 mm polyester
Line section 2 length (m)	1378.9
Line section 3 material	120 mm R4 studless chain
Line section 3 length (m)	80

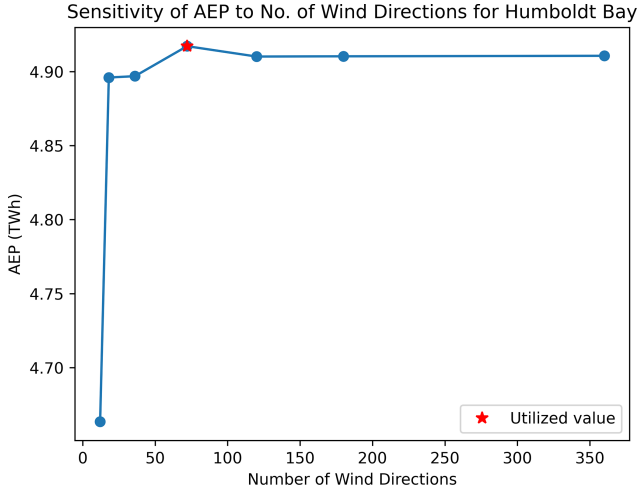

Figure 15. Humboldt Bay layout AEP sensitivity to discretization of wind directions for wind rose.

The Gulf of Maine array design uses a three-line semitaut mooring system consisting of chain and polyester with drag-embedment anchors from Lozon et al. (2025). The chain section is approximately 500 m long, and the polyester section is 200 m long, with an anchoring radius of 700 m. Table 14 details the mooring configuration.

The dynamic cable is a lazy-wave configuration, also adopted from Lozon et al. (2025). We directly implemented the 300 mm^2 cable conductor size from Lozon et al. (2025), and then we adapted the number of buoyancy modules for the larger conductors sizes. The 300 mm^2 cable includes 6 buoyancy modules over the buoyancy section, while the 630 mm^2 cable includes 10, and the 1000 mm^2 cable includes 14. All cables have a constant buoyancy section length of 60 m, meaning the buoyancy module spacing decreases as the conductor size increases. The design parameters for the three different cable conductor sizes are shown in Table 15.

3.2.3 Optimized layout

We optimized the Gulf of Maine reference array to minimize the LCOE for 132 turbines within a 504.5 km^2 area. Table 16 shows the grid transformation design variables for the Gulf of Maine optimized reference array layout. The spacing in the x direction is 1442 m, and the spacing in the y direction is 2564 m. The grid has a 180° rotation with a skew of −18°, and all turbines are rotated to 60°.

The optimized reference array layout is shown in Fig. 18.

There are two substations in this array to accommodate the larger number of turbines. The substations are located at a slight offset from the center of the farm, with one closer to the northwest corner and one closer to the southeast corner. We chose these locations prior to the optimization to reduce the lengths of cables connected in series. The optimizer then placed the substations at the grid points closest to the user-defined locations.

Each substation mooring system features eight lines, with two on each corner spaced 20° apart. One side of each substation is free of cables to allow space for a maintenance vessel to approach. The intra-array cables enter at headings spaced 5° apart for each side. The substations are rotated 25°, which is 35° less than the turbine platforms. We chose this heading after the optimization process to prevent sharp angles when rerouting the cables entering the substation. Figure 19 shows a close-up view of this rerouting on the northwest substation.

The algorithm described in Sect. 2.3.6 rerouted the dynamic cables to be at least 25° offset from the mooring line headings of their associated platforms to avoid clashing, and then it rerouted the static cables to follow the dynamic cable heading for an additional 300 m before routing toward the next platform to ensure that the mooring lines and cables would not cross.

Figure 20a visualizes the FLORIS wake model with winds at 12 $m\,s^{-1}$ from the predominant wind direction, 205° clockwise from due north. Figure 20b shows a polar plot of the wake losses for a wind speed of 12 $m\,s^{-1}$ at each angle with a 1° interval. Though some directions produce significant wake losses, the wake losses dramatically decrease with even slight changes in the wind direction. When comparing the major wake loss directions in subplot (b) to the uniform-grid layout in subplot (a), the largest wake losses are along the east–west directions at up to 35 % loss due to the small grid spacing in this direction. Figure 16a shows that the wind resource is limited in this direction, so there is limited impact on the AEP.

There are also notable wake losses in the northwest–southeast and northeast–southwest directions, which can be attributed to the cross-wise grid direction; however, these wake losses are less than 10 %. Near the predominant wind direction, there is a wake loss of less than 1 %. The layout largely avoids wake losses in directions with significant wind resource. The wind rose of the Gulf of Maine is more spread than that of Humboldt Bay, making it difficult to completely

Table 10. Dynamic power cable design parameters for Humboldt Bay.

Parameter	Value		
Conductor size (mm^2)	300	630	1000
Cable span (m)	500	500	500
Fairlead radius (m)	5	5	5
Total cable length (m)	1070.43	1070.43	1070.43
Length of cable below buoyancy section	297.98	297.98	297.98
Midpoint of buoyancy section (m)	497.98	497.81	497.98
Buoyancy section length (m)	400	400	400
Length of cable above buoyancy section (m)	372.45	372.45	372.45
Number of buoyancy modules	34	60	89
Buoyancy module spacing (m)	12.07	6.76	4.52
Averaged diameter of buoyancy section (m)	0.290	0.377	0.451
Averaged mass of buoyancy section ($kg\,m^{-1}$)	59.17	96.63	136.5

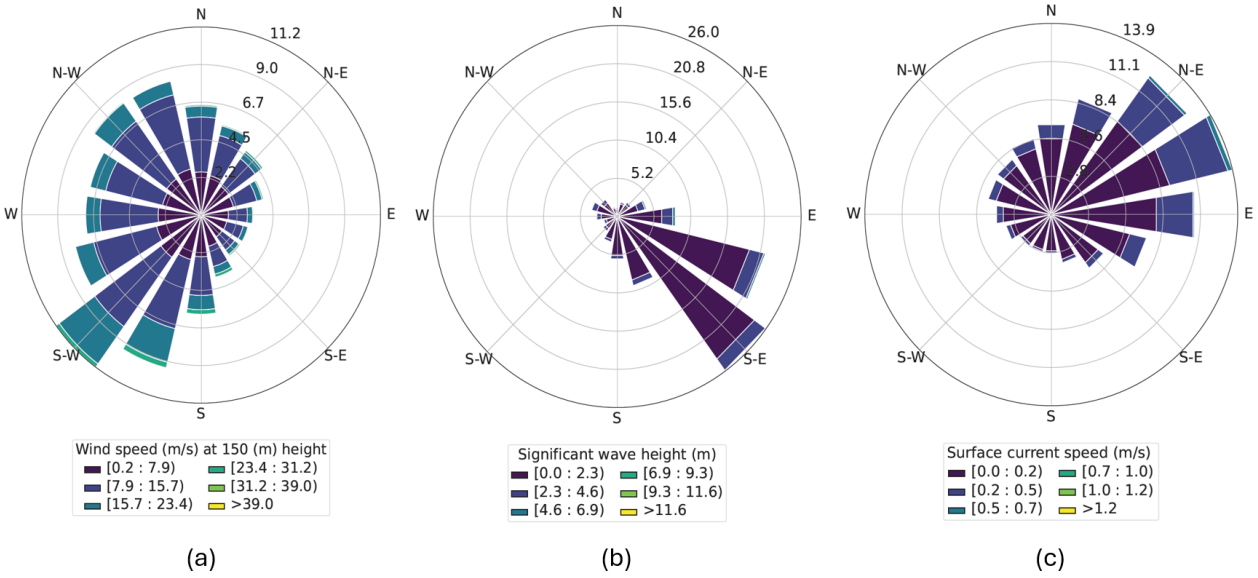

Figure 16. Gulf of Maine **(a)** wind, **(b)** wave, and **(c)** current roses (Biglu et al., 2024a).

Table 11. Humboldt Bay reference array layout design variables.

Parameter	Value
Grid x spacing, D'_x (m)	1847.2
Grid y spacing, D'_y (m)	1431.3
Grid x translation, x_0 (m)	−494.8
Grid y translation, y_0 (m)	−3552.0
Grid rotation, α (°)	36.7
Grid skew, β (°)	7.3
Platform rotation, γ (°)	3.1, 63.1

Table 12. Humboldt Bay reference array layout AEP and mooring, cable, and anchor CapEx.

Performance metric	Value
AEP (GWh)	4873
Cable CapEx ($\times 10^6$ USD)	202.2
Mooring lines CapEx ($\times 10^6$ USD)	93.8
Anchor CapEx ($\times 10^6$ USD)	66.1

avoid wake losses in all relevant wind directions. Notably, the wind rose data used to calculate AEP used 5° direction intervals to balance computational efficiency with AEP accuracy. When those same 5° intervals are used to calculate wake loss percentages, no wake losses appear in the interval covering the predominant wind direction due to the drastic decay in the wake losses around a specific angle. This suggests that a more granular wind rose discretization might be needed to better capture the wake losses in the AEP calculations within layout optimizations.

Table 13. Gulf of Maine extreme load case conditions.

Parameter	DLC 1.6	DLC 6.1	SLC
H_S (m)	7.11	11.86	14.19
T_P (s)	12.2	15.75	17.23
Current speed ($m\,s^{-1}$)	0.71	0.88	1.34
Wind speed ($m\,s^{-1}$)	10.59	40.59	42.96
Turbulence intensity	0.06	0.05	0.05

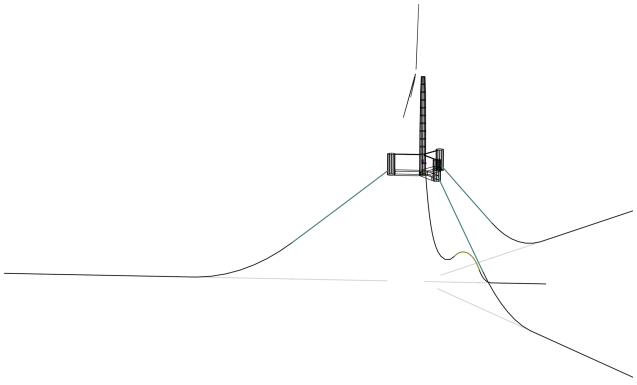

Figure 17. Gulf of Maine mooring and dynamic cable system (Lozon et al., 2025).

We repeated the AEP sensitivity analysis for the Gulf of Maine design, applying the same wind direction discretizations as in Sect. 3.1.3. The highest granularity, 360 directions, produced a 0.01 TWh (0.1 %) decrease in AEP compared to the chosen granularity (72 directions, starred in Fig. 21). Lower numbers of wind directions produced more varying results, while the chosen granularity produces an adequate result for significantly less computational expense.

The final values affecting the LCOE calculations in the optimization process are described in Table 17. These cost values reflect the final design, which includes the refined cable routing. The Gulf of Maine total anchor material costs are an order of magnitude less than the total cable material costs. The cable material costs are similar to the mooring system material costs, unlike the Humboldt Bay design. These costs are based on the cost curves in Sect. 2.3.3. The AEP, at nearly 10 TWh, is significantly larger than that of the Humboldt Bay design due to the increased number of turbines.

3.3 Gulf of America

The Gulf of America array design features catenary mooring systems and lazy-wave dynamic cables. It has 67 turbines for a total capacity of 1.005 GW. The substation, located in the center of the array, is the terminus of nine cable routes.

Table 14. Gulf of Maine mooring line design adapted from Lozon et al. (2025).

Parameter	Value
Anchoring radius (m)	700
Fairlead radius (m)	58
Fairlead depth (m)	14
Pretension (kN)	1205
Declination angle (°)	38.33
Line section 1 material	181.8 mm polyester
Line section 1 length (m)	199.8
Line section 2 material	155 mm R4 studless chain
Line section 2 length (m)	497.7

3.3.1 Site conditions

The Gulf of America has a wide range of water depths within the federal exclusive economic zone. The wind energy call area developed for the Gulf of America is mostly shallow water suitable for fixed-bottom wind turbines, but some portions are deep enough (greater than 60 m) to require floating wind (Fuchs et al., 2023). We chose a water depth of 80 m for the Gulf of America reference array. The wind, wave, and current roses are shown in Fig. 22. The extreme load cases used to evaluate the mooring and cable designs are described in Table 18. The extreme load case parameters in this reference site dataset use the same approach as the other sites in Biglu et al. (2024a). This approach, which involves fitting probability distributions to the maxima or peaks in time series data, is a simplification that is not well suited for the extreme tropical cyclone conditions that can occur in this region. Designing specifically for tropical cyclone conditions was left for future work because the intent of the reference array designs is to suit the already-defined reference site conditions.

3.3.2 Mooring and cable design

We adopted the three-line catenary chain mooring system with drag-embedment anchors and lazy-wave dynamic cables developed in Lozon et al. (2025) for use in the Gulf of America reference array. The anchoring radius is 400 m with a total line length of 364.5 m. Figure 23 shows the mooring and dynamic cable configurations used in the Gulf of America reference array.

The dynamic cables used in the Gulf of America reference array are 80 m depth lazy-wave cable designs adopted from Lozon et al. (2025). From the original optimized design for the 300 mm^2 cable conductor size, we adapted the number of buoyancy modules for the larger sizes. The 300 mm^2 cable includes 5 buoyancy modules over the buoyancy section, while the 630 mm^2 cable includes 8, and the 1000 mm^2 cable includes 12. All cables have a constant buoyancy section length of 50 m, meaning the buoyancy module spacing

Table 15. Gulf of Maine lazy-wave dynamic cable designs.

Parameter	Value		
Conductor size (mm^2)	300	630	1000
Anchor point (m)	205	205	205
Total cable length (m)	353.51	353.51	353.51
Length of cable below buoyancy section (m)	121.53	121.53	121.53
Buoyancy section length (m)	60	60	60
Midpoint of buoyancy section (m)	151.53	151.53	151.53
Length of cable above buoyancy section (m)	171.98	171.98	171.98
Number of buoyancy modules	6	10	14
Buoyancy module spacing (m)	11.23	6.38	4.53
Averaged diameter of buoyancy section (m)	0.30	0.40	0.46
Averaged mass of buoyancy section ($kg\,m^{-1}$)	60.85	103.22	140.73

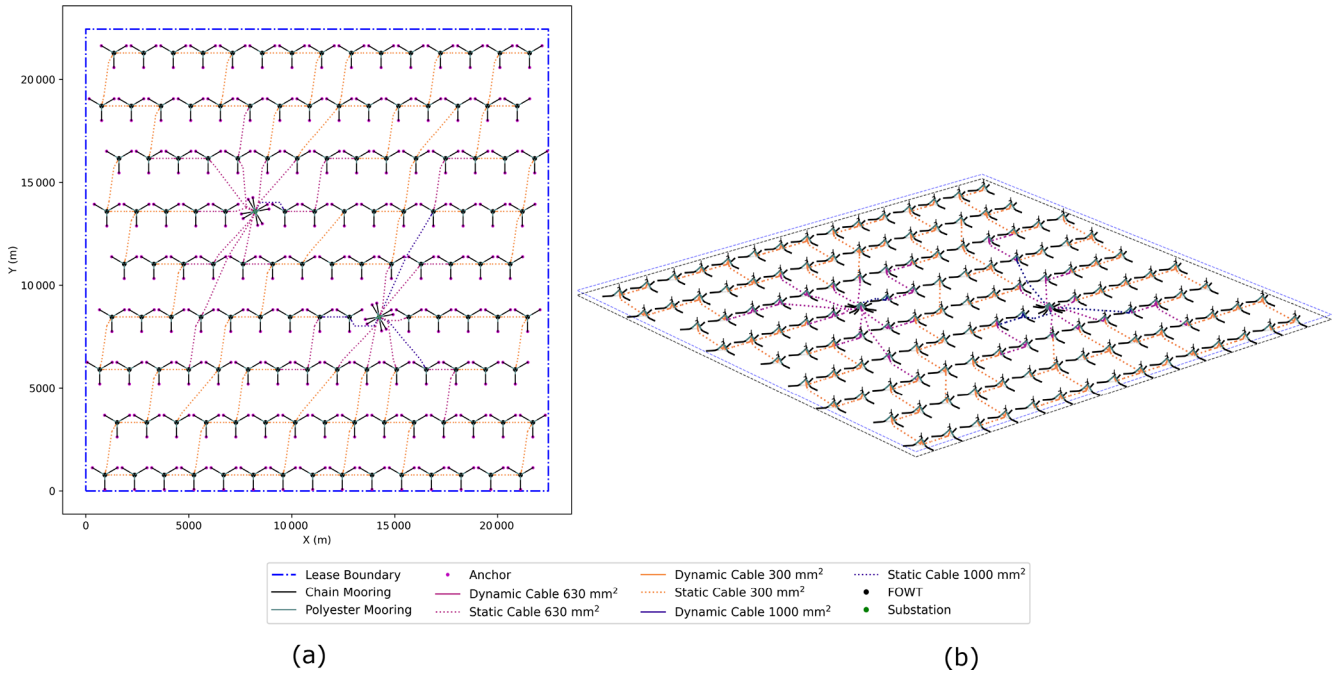

Figure 18. Gulf of Maine array layout and cable routing in **(a)** plan view and **(b)** three dimensions.

Table 16. Gulf of Maine optimized reference array layout design variables.

Parameter	Value
Grid x spacing, D'_x (m)	1442.0
Grid y spacing, D'_y (m)	2563.7
Grid x translation, x_0 (m)	−1562.2
Grid y translation, y_0 (m)	2359.9
Grid rotation, α (°)	180.0
Grid skew, β (°)	−18.3
Platform rotation, γ (°)	60.0

Table 17. Gulf of Maine reference array layout AEP and mooring, cable, and anchor CapEx.

Performance metric	Value
AEP (GWh)	9859.5
Cable CapEx ($\times 10^6$ USD)	250.9
Mooring lines CapEx ($\times 10^6$ USD)	270.7
Anchor CapEx ($\times 10^6$ USD)	21.5

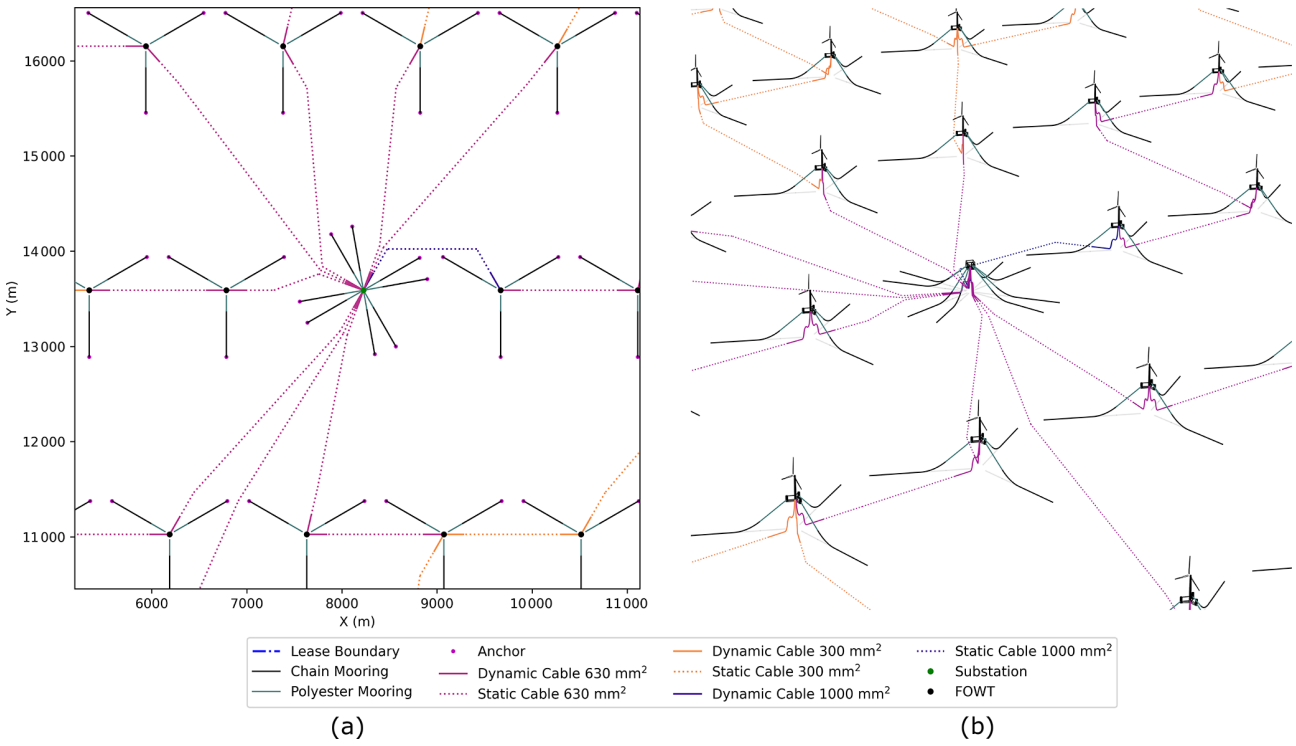

Figure 19. Final routing of intra-array cables into substation for the Gulf of Maine array in **(a)** plan view and **(b)** three dimensions.

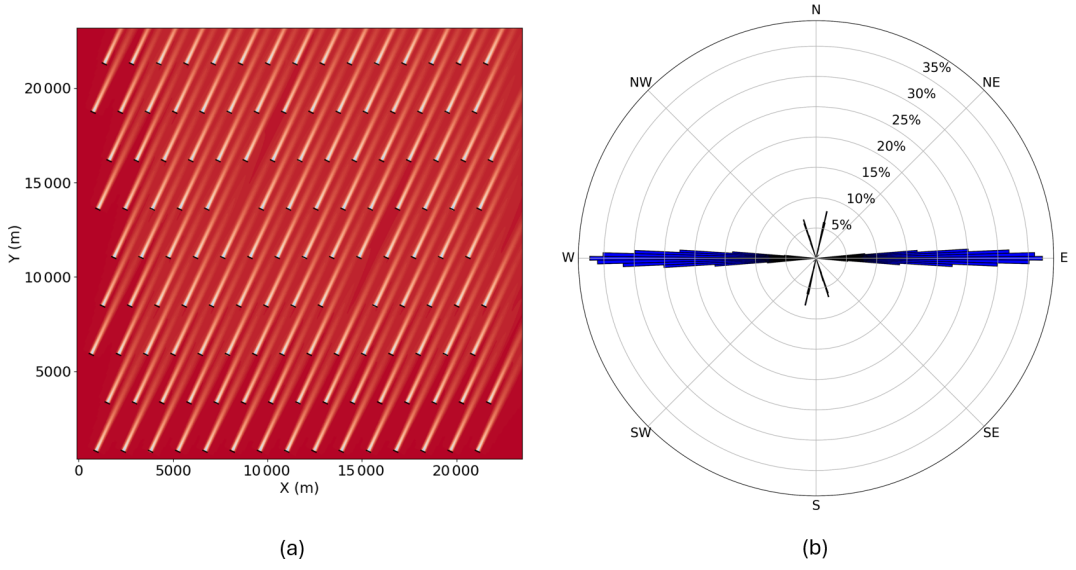

Figure 20. Gulf of Maine optimized array layout: **(a)** wakes with a wind speed of 12 m s^{-1} from the predominant wind direction and **(b)** wake losses at each direction with a wind speed of 12 m s^{-1}.

decreases as the conductor size increases. The cable design parameters are shown in Table 20.

3.3.3 Optimized layout

We optimized the Gulf of America reference array layout to minimize the LCOE for 67 turbines in a 280.7 km^2 square lease area. The layout is a uniform grid with 1189 m spacing in the x direction and 3991 m spacing in the y direction. There is no grid rotation, but there is a 6° skew. Each turbine platform has a heading of 60.3°. Table 21 shows the grid transformation variables for the Gulf of America reference array layout. The predominant southeast wind direction

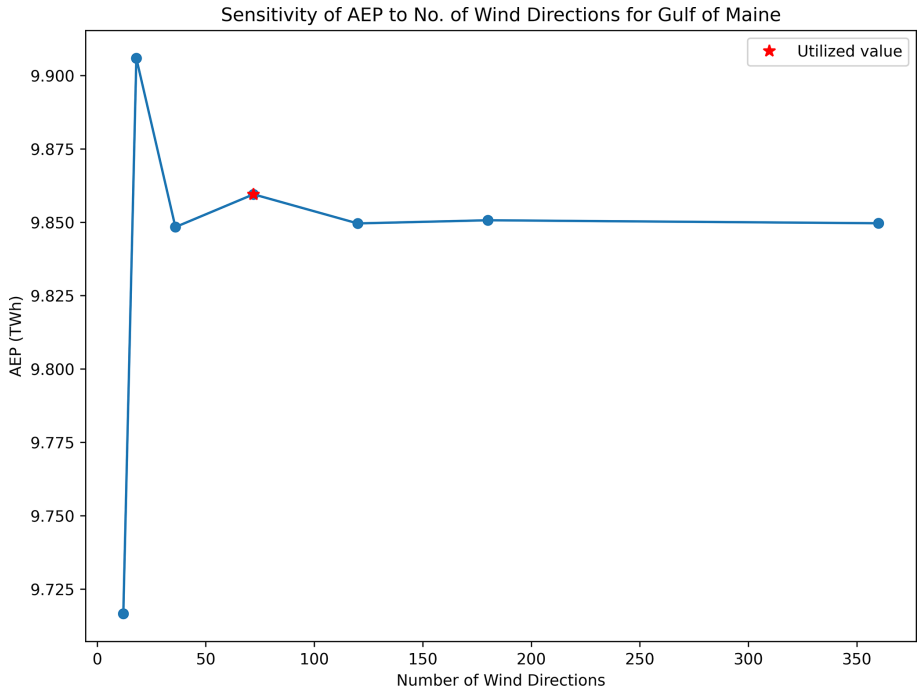

Figure 21. Gulf of Maine layout AEP sensitivity to discretization of wind directions for wind rose.

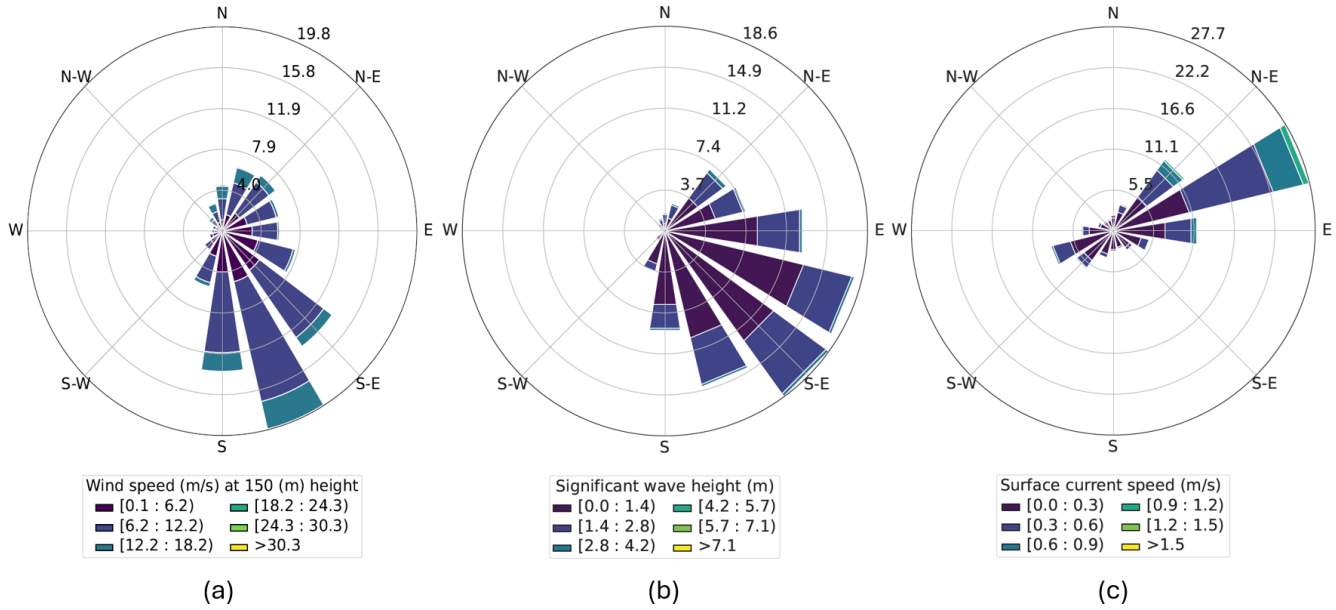

Figure 22. Gulf of America **(a)** wind, **(b)** wave, and **(c)** current roses (Biglu et al., 2024a).

led to a significantly larger spacing in the y direction than in the x direction.

The optimized layout for the Gulf of America reference array is shown in Fig. 24.

It is notable that there are extra grid locations without turbines. The location of the unused grid points is based on the optimization process's method of filling in the grid, which removes turbines closest to the lease area boundary until the correct number of turbines are remaining. It is possible that the placement of these unused grid points and the substation in another part of the grid could improve the AEP; however, these considerations are an additional variable that is out of the scope of this optimization. We placed the substation in the center of the array to reduce the cable lengths and sizes.

The substation mooring system features eight mooring lines, with two on each corner of the substation spaced 20°

Table 18. Gulf of America extreme load case conditions.

Parameter	DLC 1.6	DLC 6.1	SLC
H_S (m)	5.5	6.8	7.4
T_P (s)	10.8	11.9	12.5
Current speed ($m\,s^{-1}$)	0.71	0.88	1.34
Wind speed ($m\,s^{-1}$)	10.59	29.8	31.5
Turbulence intensity	0.06	0.05	0.05

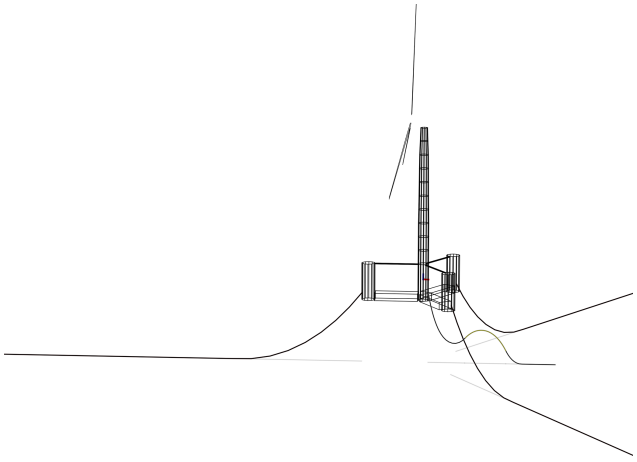

Figure 23. Gulf of America mooring and cable configuration (Lozon et al., 2025).

apart. Figure 25 provides a close-up view of the rerouting around the substation. Cables are routed to three sides, with three cables on each. In each side, cable headings entering the substation are spaced 5° apart to prevent clashing between cables. The substation is rotated 35.3°, 25° less than the turbine platforms. We chose this heading after the optimization process to prevent sharp angles when rerouting the cables entering the substation.

Figure 26a visualizes the Gulf of America FLORIS wake model with winds at $12\,m\,s^{-1}$ from the predominant southeast wind direction. Figure 26b shows a polar plot of the wake losses, where the array wake losses were calculated for every angle at an interval of 1° when the wind speed is $12\,m\,s^{-1}$. When comparing the major wake loss directions in subplot (b) to the uniform-grid layout in subplot (a), it is clear that the main wake loss directions are east–west along the x direction of the grid, as this direction affords the least distance between turbines. Comparing subplot (b) with the wind rose in Fig. 22a, the predominant southeast wind direction does not align with the major wake loss directions. Though there is significant wind coming from the south, which aligns with the y direction of the grid, there is no significant wake loss due to the large north–south spacing in the grid.

We replicated the AEP sensitivity analysis for the Gulf of America array design, with results shown in Fig. 27. The highest granularity, 360 directions, produced a 0.002 TWh (0.05 %) decrease in AEP compared to the chosen granularity (72 directions, starred in Fig. 27). Therefore, the chosen granularity produces a reasonably close AEP estimate for significantly less computational expense.

Table 19. Gulf of America mooring line design adapted from Lozon et al. (2025).

Parameter	Value
Anchoring radius (m)	400
Fairlead radius (m)	58
Fairlead depth (m)	14
Pretension (kN)	748
Declination angle (°)	52.0
Line material	160 mm R4 studless chain
Line length (m)	364.5

The final values affecting the LCOE calculations in the optimization process are described in Table 22. The cable material costs are similar to the total mooring material costs. These costs reflect the material cost of the final design, including the refined cable routing. The AEP is less than that of Humboldt Bay, which has the same total capacity, consistent with the reduced wind resource in the Gulf of America.

4 Conclusions

Floating wind reference array designs were developed for three representative regions of the United States while accounting for the site conditions of each area. Each design has a uniform-grid array layout that is optimized to approximately minimize the LCOE. The designs include three-dimensional definitions of major components and systems – such as mooring lines, anchors, dynamic cables, turbines, floating platforms, and substations – as well as the layout of these components and the routing of the static array cables.

The design approach combines the adaptation of the existing component designs and the optimization of the array layout along with additional fine-tuning steps. All designs use the common VolturnUS-S 15 MW reference floating wind turbine system and an existing floating substation design. Reference mooring lines, dynamic cables, and anchors were adopted from previous work. We adapted the dynamic cable designs for the larger conductor sizes needed by these arrays. We developed an array layout methodology that built upon previous work to improve efficiency, integrate substations in the uniform grid, and route to multiple substations in an array optimization. Spatial constraints were used to ensure the output array design was feasible. Intra-array cable routing was developed using three different conductor sizes for the unique layout of each array. Further routing adjustments were made with an algorithm developed to prevent cables from clashing with moorings and anchors, and manual adjustments were made to connect the intra-array dynamic

Table 20. Gulf of America lazy-wave dynamic cable designs.

Parameter	Value		
Conductor size (mm^2)	300	630	1000
Anchor point (m)	125	125	125
Total cable length (m)	170.215	170.215	170.215
Length of cable below buoyancy section (m)	52.101	52.101	52.101
Buoyancy section length (m)	50	50	50
Midpoint of buoyancy section (m)	77.1	77.1	77.1
Length of cable above buoyancy section (m)	68.114	68.114	68.114
Number of buoyancy modules	5	8	12
Buoyancy module spacing (m)	11.88	7.23	4.59
Averaged diameter of buoyancy section (m)	0.290	0.386	0.463
Averaged mass of buoyancy section ($kg\,m^{-1}$)	59.53	99.09	140.83

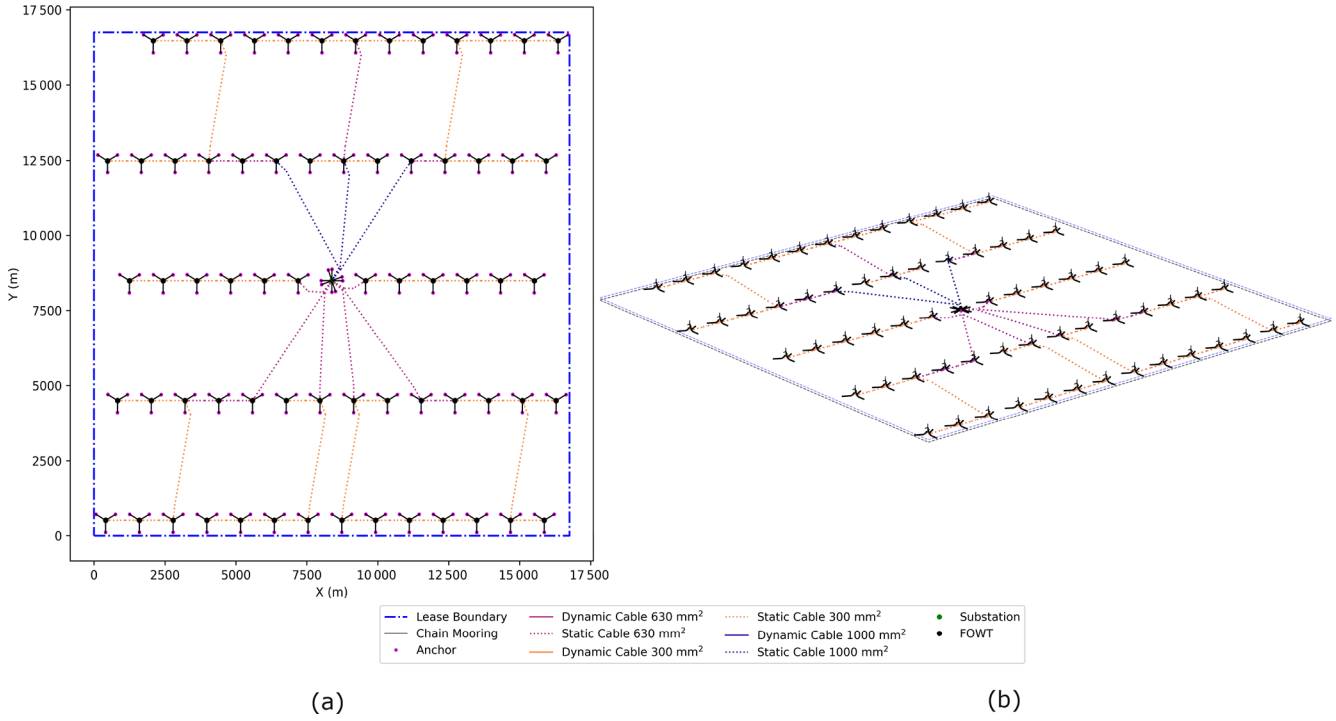

Figure 24. Gulf of America array layout and cable routing in **(a)** plan view and **(b)** three dimensions.

Table 21. Gulf of America optimized reference array layout design variables.

Parameter	Value
Grid x spacing (m)	1188.9
Grid y spacing (m)	3991.2
Grid x translation (m)	−414.7
Grid y translation (m)	−3878.1
Grid rotation (°)	0.0
Grid skew (°)	6.0
Platform rotation (°)	60.3

Table 22. Gulf of America reference array layout AEP and mooring, cable, and anchor CapEx.

Performance metric	Value
AEP (GWh)	3681.9
Cable CapEx ($\times 10^6$ USD)	112.5
Mooring lines CapEx ($\times 10^6$ USD)	100.8
Anchor CapEx ($\times 10^6$ USD)	13.2

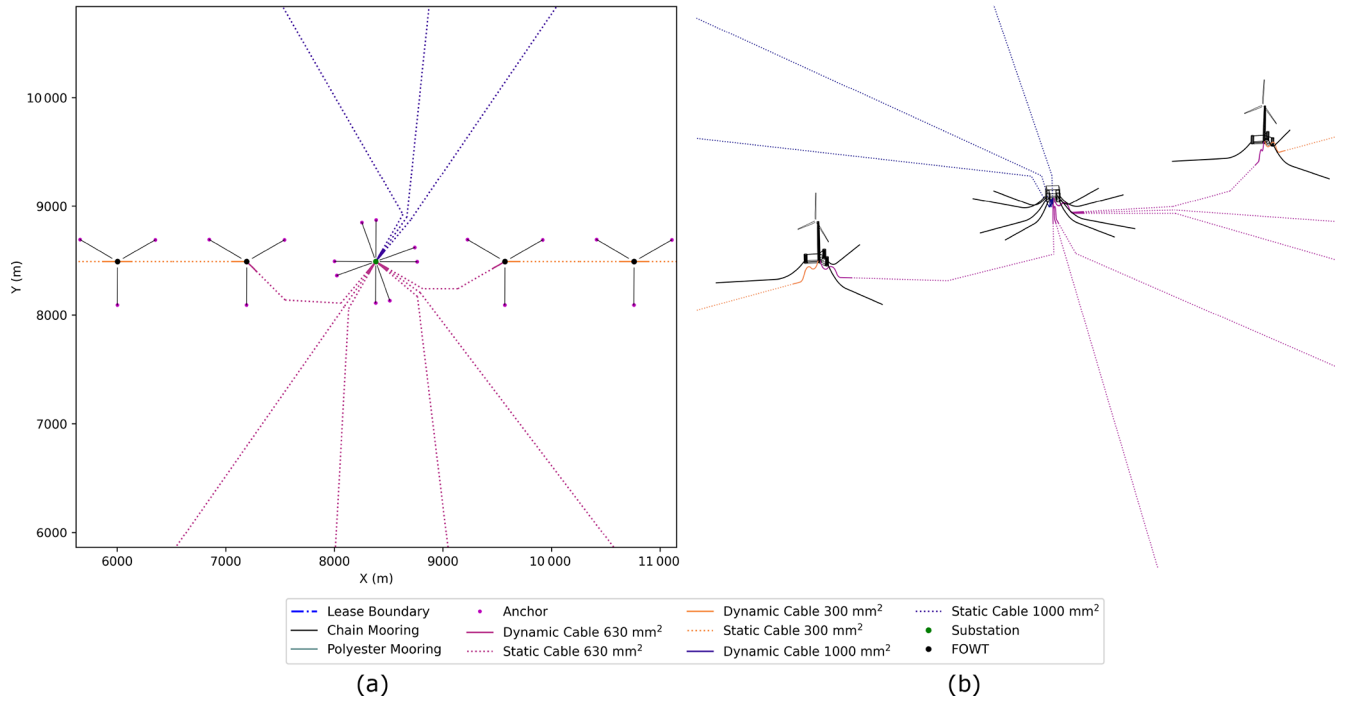

Figure 25. Final routing of intra-array cables into substation for the Gulf of America array in **(a)** plan view and **(b)** three dimensions.

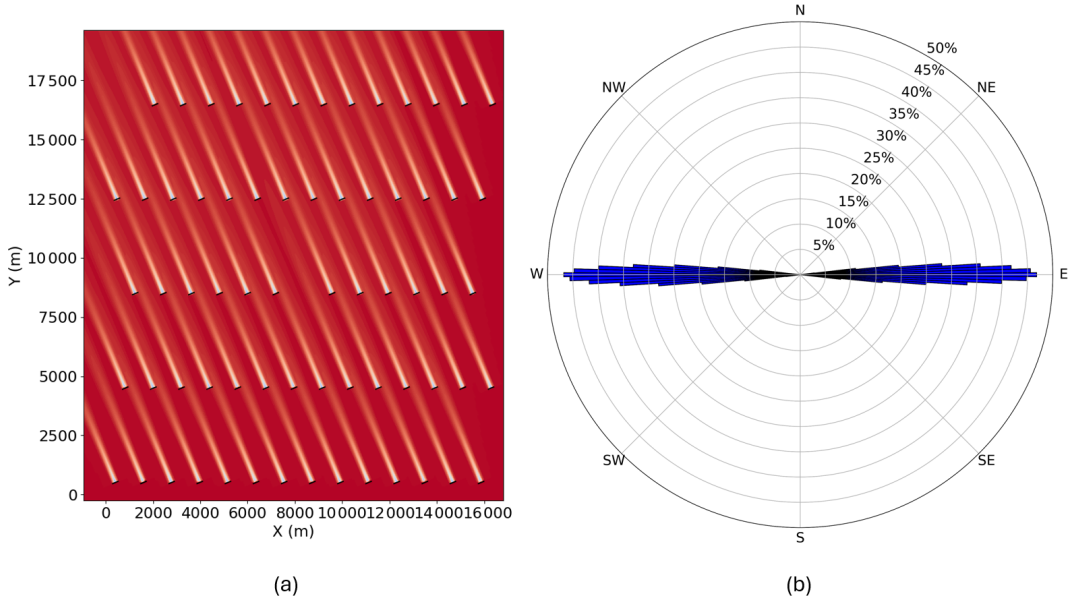

Figure 26. Gulf of America optimized array layout: **(a)** wakes with a wind speed of 12 m s^{-1} from the predominant wind direction and **(b)** percent wake losses with a wind speed of 12 m s^{-1} at each wind heading direction.

cables to the substation at 5° intervals. These cable routing adjustment techniques create more realistic cable routing in the array layout designs. We confirmed the layout optimality of each array by checking the wake losses at each wind heading, and we found that the arrays largely avoid wake losses in the predominant wind directions.

The reference designs, and especially their optimized array layouts, provide examples of effective design characteristics for each region. The Humboldt Bay design uses taut mooring systems for cost efficiency in deep water. The large anchoring radius necessitates similar turbine spacings in each direction, despite the very directional wind resource. Wake

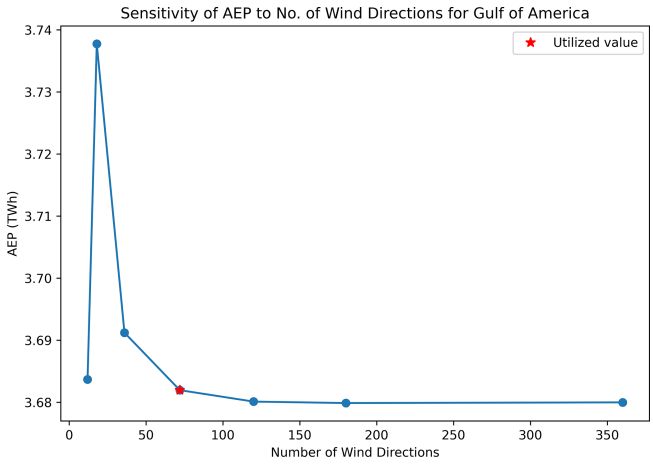

Figure 27. Gulf of America layout AEP sensitivity to discretization of wind directions for wind rose.

losses are instead minimized by orienting the array layout at a diagonal to the predominant wind direction. The Gulf of Maine design uses semitaut mooring systems for cost efficiency in moderate water depths. Given the larger size of the proposed lease areas in the Gulf of Maine, we used a larger array capacity and two substations. The Gulf of Maine wind resource is relatively spread compared to Humboldt Bay, requiring avoidance of wake losses in multiple different directions. The wake losses are minimized with a larger y spacing and a significant grid skew angle. The Gulf of America design uses catenary mooring systems due to the shallow depth. The fairly directional wind resource and small anchoring radius allowed platforms to be tightly packed in the x direction, leaving large spacing in the y direction to avoid wake losses in the dominant wind direction.

The three reference designs are described in detail by publicly available design definition files, making the designs available for use in floating wind research and development projects where array-level scenarios are needed. These reference designs can serve as baselines for evaluating various floating wind innovations at the array scale or comparing with commercial-scale floating wind array designs. The designs can also be built upon or adapted, with portions of the design substituted to fit different locations, requirements, and research focuses.

The scope of the presented reference design methodology is limited to approximately optimizing uniform-grid array layouts of selected floating turbine systems, including power cable design and layout, with a representative wind rose, lease area, water depth, and soil type for each region. Spatial constraints account for navigability and potential component clashing. Though this methodology was carefully chosen to yield practical reference designs for a variety of purposes, there are a few clear limitations to the presented approach. One limitation is the relatively coarse discretization of the wind rose directions, which was found to not capture all relevant wake losses due to their specific directionality. Another limitation is the superficial analysis of the optimization approach performance; although the layouts perform well, it is likely that the optimizer did not find the true global minimum LCOE. Further, some highly site-specific factors relevant to commercial-scale floating wind array designs, such as grid interconnection details, were not in the scope of these reference designs.

Future work could evaluate the reference designs for many real-world factors that were not considered in detail for the presented methodology, such as varied bathymetry and sediment, export cable routing, installation, maintenance, and supply chain availability. The designs can be applied and altered as necessary for a specific location within the region; for example, the mooring and cable designs used in the present work can be used as a standardized baseline design to be altered for site-specific bathymetry. Mooring designs can be adapted for small changes in water depth by increasing section lengths while maintaining horizontal pretension, and dynamic cable designs can be adapted for bathymetry by increasing cable length and adjusting buoyancy sections to maintain cable profile. The scope of the reference design approach could be expanded to consider these drivers for a more holistic design. For example, installation and maintenance techniques can be simulated and optimized for these layout designs, and constraints or estimations can be added to the design methodology to consider these factors in future array layout optimizations. Optimization approaches and settings can be compared and adjusted to achieve a more optimal or faster optimization.

Appendix A: Humboldt Bay platform positions

The Humboldt Bay array layout platform positions are listed in Table A1. The mooring orientation is counterclockwise relative to a mooring line due north for turbines. For substations, the mooring orientation is relative to one pontoon facing each cardinal direction.

Table A1. Humboldt Bay array layout platform positions.

Platform	x position	y position	Orientation (°)
Turbine 1	9051	9170	3
Turbine 2	8278	6809	63
Turbine 3	6861	9323	63
Turbine 4	9759	7913	63
Turbine 5	6088	6962	3
Turbine 6	6797	5705	63
Turbine 7	8342	10 427	63
Turbine 8	8986	5552	3
Turbine 9	10 467	6656	3
Turbine 10	10 532	10 274	3
Turbine 11	6153	10 580	3
Turbine 12	5380	8219	63
Turbine 13	11 176	5399	63
Turbine 14	11 240	9017	63
Turbine 15	4672	9476	3
Turbine 16	4607	5858	3
Turbine 17	5316	4601	63
Turbine 18	9823	11 531	63
Turbine 19	7505	4448	3
Turbine 20	7634	11 684	3
Turbine 21	9695	4295	63
Turbine 22	5444	11 837	63
Turbine 23	11 884	4142	3
Turbine 24	11 949	7760	3
Turbine 25	12 013	11 378	3
Turbine 26	3963	10 733	63
Turbine 27	3899	7115	63
Turbine 28	3835	3497	63
Turbine 29	11 304	12 635	63
Turbine 30	6024	3344	3
Turbine 31	12 657	6503	63
Turbine 32	12 721	10 121	63
Turbine 33	3255	11 990	3
Turbine 34	9115	12 788	3
Turbine 35	8214	3191	63
Turbine 36	3190	8372	3
Turbine 37	3126	4754	3
Turbine 38	6925	12 941	63
Turbine 39	10 403	3038	3
Turbine 40	4736	13 094	3
Turbine 41	12 593	2885	63
Turbine 42	13 365	5246	3
Turbine 43	13 430	8864	3
Turbine 44	2546	13 247	63
Turbine 45	13 494	12 482	3
Turbine 46	2482	9629	63
Turbine 47	2418	6011	63
Turbine 48	2354	2393	63
Turbine 49	12 785	13 739	63
Turbine 50	4543	2240	3
Turbine 51	10 596	13 892	3
Turbine 52	6733	2087	63
Turbine 53	8406	14 045	63
Turbine 54	8922	1934	3
Turbine 55	14 074	3989	63
Turbine 56	14 138	7606	63
Turbine 57	6217	14 198	3
Turbine 58	14 202	11 224	63
Turbine 59	11 112	1781	63
Turbine 60	1774	10 886	3
Turbine 61	1709	7268	3
Turbine 62	4027	14 351	63
Turbine 63	1645	3651	3
Turbine 64	13 301	1628	3
Turbine 65	1838	14 504	3
Turbine 66	14 782	2731	3
Turbine 67	14 267	14 842	63
Substation	7569	8066	3

Appendix B: Gulf of Maine platform positions

The Gulf of Maine array layout platform positions are listed in Table B1. The mooring orientation is counterclockwise relative to a mooring line due north for turbines. For substations, the mooring orientation is relative to one pontoon facing each cardinal direction.

Table B1. Gulf of Maine array layout platform positions.

Platform	x position	y position	Orientation (°)
Turbine 1	21 549	21 282	60
Turbine 2	20 107	21 282	60
Turbine 3	18 665	21 282	60
Turbine 4	17 223	21 282	60
Turbine 5	15 781	21 282	60
Turbine 6	14 339	21 282	60
Turbine 7	12 897	21 282	60
Turbine 8	11 455	21 282	60
Turbine 9	10 013	21 282	60
Turbine 10	8571	21 282	60
Turbine 11	7129	21 282	60
Turbine 12	5687	21 282	60
Turbine 13	4245	21 282	60
Turbine 14	2803	21 282	60
Turbine 15	1361	21 282	60
Turbine 16	20 953	18 718	60
Turbine 17	19 511	18 718	60
Turbine 18	18 069	18 718	60
Turbine 19	16 627	18 718	60
Turbine 20	15 185	18 718	60
Turbine 21	13 743	18 718	60
Turbine 22	12 301	18 718	60
Turbine 23	10 859	18 718	60
Turbine 24	9418	18 718	60
Turbine 25	7976	18 718	60
Turbine 26	6534	18 718	60
Turbine 27	5092	18 718	60
Turbine 28	3650	18 718	60
Turbine 29	2208	18 718	60
Turbine 30	766	18 718	60
Turbine 31	21 800	16 154	60
Turbine 32	20 358	16 154	60
Turbine 33	18 916	16 154	60
Turbine 34	17 474	16 154	60
Turbine 35	16 032	16 154	60
Turbine 36	14 590	16 154	60
Turbine 37	13 148	16 154	60
Turbine 38	11 706	16 154	60
Turbine 39	10 264	16 154	60
Turbine 40	8822	16 154	60
Turbine 41	7380	16 154	60
Turbine 42	5938	16 154	60
Turbine 43	4496	16 154	60
Turbine 44	3054	16 154	60
Turbine 45	1612	16 154	60
Turbine 46	21 204	13 590	60
Turbine 47	19 762	13 590	60
Turbine 48	18 320	13 590	60
Turbine 49	16 878	13 590	60
Turbine 50	15 436	13 590	60
Turbine 51	13 994	13 590	60
Turbine 52	12 552	13 590	60
Turbine 53	11 110	13 590	60
Turbine 54	9668	13 590	60
Turbine 55	6784	13 590	60
Turbine 56	5342	13 590	60
Turbine 57	3900	13 590	60
Turbine 58	2458	13 590	60
Turbine 59	1016	13 590	60
Turbine 60	20 609	11 027	60
Turbine 61	19 167	11 027	60
Turbine 62	17 725	11 027	60
Turbine 63	16 283	11 027	60
Turbine 64	14 841	11 027	60
Turbine 65	13 399	11 027	60
Turbine 66	11 957	11 027	60
Turbine 67	10 515	11 027	60
Turbine 68	9073	11 027	60
Turbine 69	7631	11 027	60
Turbine 70	6189	11 027	60
Turbine 71	4747	11 027	60
Turbine 72	3305	11 027	60
Turbine 73	1863	11 027	60
Turbine 74	21 455	8463	60
Turbine 75	20 013	8463	60
Turbine 76	18 571	8463	60
Turbine 77	17 129	8463	60
Turbine 78	15 687	8463	60
Turbine 79	12 803	8463	60
Turbine 80	11 361	8463	60
Turbine 81	9919	8463	60
Turbine 82	8477	8463	60
Turbine 83	7035	8463	60
Turbine 84	5593	8463	60
Turbine 85	4151	8463	60
Turbine 86	2709	8463	60
Turbine 87	1267	8463	60
Turbine 88	20 859	5899	60
Turbine 89	19 417	5899	60
Turbine 90	17 975	5899	60
Turbine 91	16 533	5899	60
Turbine 92	15 091	5899	60
Turbine 93	13 650	5899	60
Turbine 94	12 208	5899	60
Turbine 95	10 766	5899	60

Table B1. Continued.

Platform	x position	y position	Orientation (°)
Turbine 96	9324	5899	60
Turbine 97	7882	5899	60
Turbine 98	6440	5899	60
Turbine 99	4998	5899	60
Turbine 100	3556	5899	60
Turbine 101	2114	5899	60
Turbine 102	672	5899	60
Turbine 103	21 706	3335	60
Turbine 104	20 264	3335	60
Turbine 105	18 822	3335	60
Turbine 106	17 380	3335	60
Turbine 107	15 938	3335	60
Turbine 108	14 496	3335	60
Turbine 109	13 054	3335	60
Turbine 110	11 612	3335	60
Turbine 111	10 170	3335	60
Turbine 112	8728	3335	60
Turbine 113	7286	3335	60
Turbine 114	5844	3335	60
Turbine 115	4402	3335	60
Turbine 116	2960	3335	60
Turbine 117	1518	3335	60
Turbine 118	21 110	772	60
Turbine 119	19 668	772	60
Turbine 120	18 226	772	60
Turbine 121	16 784	772	60
Turbine 122	15 342	772	60
Turbine 123	13 900	772	60
Turbine 124	12 458	772	60
Turbine 125	11 016	772	60
Turbine 126	9574	772	60
Turbine 127	8132	772	60
Turbine 128	6690	772	60
Turbine 129	5248	772	60
Turbine 130	3806	772	60
Turbine 131	2364	772	60
Turbine 132	923	772	60
Substation 1	8226	13 590	25
Substation 2	14 245	8463	25

Appendix C: Gulf of America platform positions

The Gulf of America array layout turbine positions are listed in Table C1. The mooring orientation is counterclockwise relative to a mooring line due north.

Table C1. Gulf of America array layout platform positions.

Platform	x position	y position	Orientation (°)
Turbine 1	411	508	60
Turbine 2	1599	508	60
Turbine 3	2788	508	60
Turbine 4	3977	508	60
Turbine 5	5166	508	60
Turbine 6	6355	508	60
Turbine 7	7544	508	60
Turbine 8	8733	508	60
Turbine 9	9922	508	60
Turbine 10	11 111	508	60
Turbine 11	12 300	508	60
Turbine 12	13 488	508	60
Turbine 13	14 677	508	60
Turbine 14	15 866	508	60
Turbine 15	830	4500	60
Turbine 16	2018	4500	60
Turbine 17	3207	4500	60
Turbine 18	4396	4500	60
Turbine 19	5585	4500	60
Turbine 20	6774	4500	60
Turbine 21	7963	4500	60
Turbine 22	9152	4500	60
Turbine 23	10 341	4500	60
Turbine 24	11 530	4500	60
Turbine 25	12 719	4500	60
Turbine 26	13 907	4500	60
Turbine 27	15 096	4500	60
Turbine 28	16 285	4500	60
Turbine 29	1249	8491	60
Turbine 30	2437	8491	60
Turbine 31	3626	8491	60
Turbine 32	4815	8491	60
Turbine 33	6004	8491	60
Turbine 34	7193	8491	60
Turbine 35	9571	8491	60
Turbine 36	10 760	8491	60
Turbine 37	11 949	8491	60
Turbine 38	13 138	8491	60
Turbine 39	14 326	8491	60
Turbine 40	15 515	8491	60
Turbine 41	479	12 482	60
Turbine 42	1668	12 482	60
Turbine 43	2857	12 482	60
Turbine 44	4045	12 482	60
Turbine 45	5234	12 482	60

Table C1. Continued.

Platform	x position	y position	Orientation (°)
Turbine 46	6423	12 482	60
Turbine 47	7612	12 482	60
Turbine 48	8801	12 482	60
Turbine 49	9990	12 482	60
Turbine 50	11 179	12 482	60
Turbine 51	12 368	12 482	60
Turbine 52	13 557	12 482	60
Turbine 53	14 745	12 482	60
Turbine 54	15 934	12 482	60
Turbine 55	2087	16 473	60
Turbine 56	3276	16 473	60
Turbine 57	4464	16 473	60
Turbine 58	5653	16 473	60
Turbine 59	6842	16 473	60
Turbine 60	8031	16 473	60
Turbine 61	9220	16 473	60
Turbine 62	10 409	16 473	60
Turbine 63	11 598	16 473	60
Turbine 64	12 787	16 473	60
Turbine 65	13 976	16 473	60
Turbine 66	15 164	16 473	60
Turbine 67	16 353	16 473	60
Substation 1	8382	8491	35

Data availability. Complete reference array design descriptions, along with links to site conditions for the three regions, are available at https://github.com/FloatingArrayDesign/ReferenceDesigns (last access: 16 March 2026) and https://doi.org/10.5281/zenodo.19055044 (Sirkis et al., 2026). The arrays are described using the IEA Wind Task 49 Ontology.

Author contributions. Leah Sirkis, Ericka Lozon, and Matthew Hall developed the methodology and wrote, edited, and reviewed the manuscript. Leah Sirkis and Ericka Lozon performed case studies, analysis, data curation, and visualization. Matthew Hall contributed to supervision, project administration, funding acquisition, and conceptualization.

Competing interests. The contact author has declared that none of the authors has any competing interests.

Disclaimer. The views expressed in the article do not necessarily represent the views of the DOE or the U.S. Government.

Publisher's note: Copernicus Publications remains neutral with regard to jurisdictional claims made in the text, published maps, institutional affiliations, or any other geographical representation in this paper. The authors bear the ultimate responsibility for providing appropriate place names. Views expressed in the text are those of the authors and do not necessarily reflect the views of the publisher.

Acknowledgements. A portion of this research was performed using computational resources sponsored by the U.S. Department of Energy's Office of Energy Efficiency and Renewable Energy and located at the National Laboratory of the Rockies.

Financial support. Funding provided by U.S. Department of Energy Energy Efficiency and Renewable Energy Wind Energy Technologies Office.

Review statement. This paper was edited by Maurizio Collu and reviewed by three anonymous referees.

References

Allen, C., Viscelli, A., Dagher, H., Goupee, A., Gaertner, E., Abbas, N., Hall, M., and Barter, G.: Definition of the UMaine VolturnUS-S reference platform developed for the IEA wind 15-megawatt offshore reference wind turbine, Tech. rep., National Renewable Energy Laboratory (NREL), Golden, CO (United States), Univ. of Maine, https://doi.org/10.2172/1660012, 2020.

Bak, C., Zahle, F., Bitsche, R., Kim, T., Yde, A., Henriksen, L. C., Hansen, M. H., Blasques, J. P. A. A., Gaunaa, M., and Natarajan, A.: The DTU 10-MW Reference Wind Turbine, in: Danish Wind Power Research 2013, Trinity, Fredericia, Denmark, https://backend.orbit.dtu.dk/ws/portalfiles/portal/55645274/The_DTU_10MW_Reference_Turbine_Christian_Bak.pdf (last access: 10 October 2025), 2013.

Bak, T., Graham, A., Sapronova, A., Florian, M., Dalsgaard Sørensen, J., Knudsen, T., Hou, P., and Chen, Z.: Baseline layout and design of a 0.8 GW reference wind farm in the North Sea, Wind Energy, 20, 1665–1683, https://doi.org/10.1002/we.2116, 2017.

Biglu, M., Hall, M., Lozon, E., and Housner, S.: Reference Site Conditions for Floating Wind Arrays in the United States, Tech. Rep. NREL/TP-5000-89897, Golden, CO, National Renewable Energy Laboratory, https://www.nrel.gov/docs/fy24osti/89897.pdf (last access: 10 October 2025), 2024a.

Biglu, M., Hall, M., Lozon, E., and Housner, S.: Reference Site Condition Datasets for Floating Wind Arrays in the United States, artwork Size: 4 files Pages: 4 files, National Renewable Energy Laboratory, Golden, CO, https://doi.org/10.7799/2425969, 2024b.

Cooperman, A., Duffy, P., Hall, M., Lozon, E., Shields, M., and Musial, W.: Assessment of Offshore Wind Energy Leasing Areas for Humboldt and Morro Bay Wind Energy Areas, California, Tech. rep., National Renewable Energy Laboratory (NREL), Golden, CO (United States), https://www.nrel.gov/docs/fy22osti/82341.pdf (last access: 5 February 2026), 2022.

Davies, R., Baca, E., and Hall, M.: An Updated Mooring Cost Modeling Tool Set with Application to a Reference Model Wave Energy Converter, Proceedings of the ASME 2025 44th International Conference on Ocean, Offshore, and Arctic Engi-

neering, ASME (American Society of Mechanical Engineers), https://doi.org/10.1115/OMAE2025-156384, 2025.

Eikrem, K. S., Lorentzen, R. J., Faria, R., Stordal, A. S., and Godard, A.: Offshore wind farm layout optimization using ensemble methods, Renew. Energ., 216, https://doi.org/10.1016/j.renene.2023.119061, 2023.

Fuchs, R., Musial, W., Zuckerman, G., Chetan, M., Marquis, M., Rese, L., Cooperman, A., Duffy, P., Green, R., Beiter, P., Hernando, D. M., Morris, Jr., J. A., Randall, A., Jossart, J. A., Mudd, L., and Vickery, P.: Assessment of Offshore Wind Energy Opportunities and Challenges in the U.S. Gulf of Mexico, Tech. Rep. NREL/TP-5000-88195, National Renewable Energy Lab. (NREL), Golden, CO (United States), https://docs.nrel.gov/docs/fy24osti/88195.pdf (last access: 5 February 2026), 2023.

Gaertner, E., Rinker, J., Sethuraman, L., Zahle, F., Anderson, B., Barter, G. E., Abbas, N. J., Meng, F., Bortolotti, P., Skrzypinski, W., et al.: IEA wind TCP task 37: definition of the IEA 15-megawatt offshore reference wind turbine, Tech. rep., National Renewable Energy Laboratory (NREL), Golden, CO (United States), https://doi.org/10.2172/1603478, 2020.

Gebraad, P., Fleming, P., Ning, S. A., and van Wingerden, J.-W.: FLORIS, https://www.osti.gov/biblio/1262644 (last access: 5 February 2026), 2014.

Green, J., Bowen, A., Fingersh, L. J., and Wan, Y.-H.: Electrical Collection and Transmission Systems for Offshore Wind Power, in: 2007 Offshore Technology Conference, OnePetro, Houston, TX, https://docs.nrel.gov/docs/fy07osti/41135.pdf (last access: 5 February 2026), 2007.

Hall, M.: Generalized Quasi-Static Mooring System Modeling with Analytic Jacobians, Energies, 17, 3155, https://doi.org/10.3390/en17133155, 2024.

Hall, M., Housner, S., Zalkind, D., Bortolotti, P., Ogden, D., and Barter, G.: An Open-Source Frequency-Domain Model for Floating Wind Turbine Design Optimization, J. Phys. Conf. Ser., 2265, 042020, https://doi.org/10.1088/1742-6596/2265/4/042020, 2022a.

Hall, M., Lozon, E., Housner, S., and Sirnivas, S.: Design and analysis of a ten-turbine floating wind farm with shared mooring lines, Proceedings of the EERA DeepWind Conference, IOP Publishing, https://doi.org/10.1088/1742-6596/2362/1/012016, 2022b.

Hall, M., Biglu, M., Housner, S., Coughlan, K., Mahfouz, M. Y., and Lozon, E.: Floating Wind Farm Layout Optimization Considering Moorings and Seabed Variations, J. Phys. Conf. Ser., 2767, 062038, https://doi.org/10.1088/1742-6596/2767/6/062038, 2024a.

Hall, M., Lozon, E., Devoy McAuliffe, F., Baudino Bessone, M., Bayati, I., Bowie, M., Bozonnet, P., Castagne, M., Feng, J., Housner, S., Janocha, M. J., Jiang, Z., Kim, Y. Y., Ko, D., Kolle, K., Lee, C. F., Lekkala, M. R., Liang, G., Mahfouz, M. Y., Mohan, M., O'Connell, D., Ong, M. C., Prieur, J., Rajasree, V. R. N., Schnepf, A., Snedker, T., Thurston-Keller, J., and Wright, C.: The IEA Wind Task 49 Reference Floating Wind Array Design Basis, Tech. Rep. NREL/TP-5000-89709, National Renewable Energy Laboratory (NREL), Golden, CO (United States), https://doi.org/10.2172/2382797, 2024b.

Hietanen, A. I., Snedker, T. H., Dykes, K., and Bayati, I.: A novel techno-economical layout optimization tool for floating wind farm design, Wind Energ. Sci., 9, 417–438, https://doi.org/10.5194/wes-9-417-2024, 2024.

Housner, S. and Mulas Hernando, D.: Levelized Cost of Energy Comparison of Floating Wind Farms With and Without Shared Anchors, NREL, Technical Report, NREL/TP-5000-89121, 2024.

ISO: ISO 19901-7: 2006: Petroleum and natural gas industries – Specific requirements for offshore structures – Part 7: Stationkeeping systems for floating offshore structures and mobile offshore units, https://www.iso.org/standard/59298.html (last access: 21 April 2026), 2005.

Janocha, M. J., Ong, M. C., Lee, C. F., Chen, K., and Ye, N.: Reference Power Cable Models for Floating Offshore Wind Applications, Sustainability, 16, 2899, https://doi.org/10.3390/su16072899, 2024.

Jonkman, B., Mudafort, R. M., Platt, A., Branlard, E., Sprague, M., Ross, H., jjonkman, HaymanConsulting, Hall, M., Slaughter, D., Vijayakumar, G., Buhl, M., Russell9798, Bortolotti, P., reos rcrozier, Ananthan, S., S, M., Rood, J., rdamiani, nrmendoza, sinolonghai, pschuenemann, ashesh2512, kshaler, Housner, S., psakievich, Bendl, K., Carmo, L., Quon, E., and mattrphillips: OpenFAST/openfast: v3.5.0, Zenodo, https://doi.org/10.5281/zenodo.7942867, 2023.

Jonkman, J. M.: Definition of the Floating System for Phase IV of OC3, Technical Report 47535, National Renewable Energy Laboratory, Golden, Colorado, https://doi.org/10.2172/979456, 2010.

Jonkman, J. M., Butterfield, S., Musial, W., and Scott, G.: Definition of a 5-MW Reference Wind Turbine for Offshore System Development, Tech. Rep. 38060, National Renewable Energy Laboratory, Golden, Colorado, https://doi.org/10.2172/947422, 2009.

Jorge Alcantara, F.: Design of a Floating Foundation for an HVAC Offshore Substation, PhD thesis, Universite de Liege, Belgium, http://hdl.handle.net/2268.2/19338 (last access: 21 April 2026), 2023.

Kainz, S., Quick, J., Souza de Alencar, M., Sanchez Perez Moreno, S., Dykes, K., Bay, C., Zaaijer, M., and Bortolotti, P.: The IEA Wind 740-10-MW Reference Offshore Wind Plants, Tech. rep., International Energy Agency Wind TCP, https://doi.org/10.2172/2333634, 2024.

Kennedy, J. and Eberhart, R.: Particle swarm optimization, in: Proceedings of ICNN'95 – International Conference on Neural Networks, IEEE, Vol. 4, 1942–1948, https://doi.org/10.1109/ICNN.1995.488968, 1995.

Kirkeby, H. and Tande, J. O.: The NOWITECH Reference Wind Farm, Enrgy. Proced., 53, 300–312, https://doi.org/10.1016/j.egypro.2014.07.239, 2014.

Lerch, M., De-Prada-Gil, M., and Molins, C.: A metaheuristic optimization model for the inter-array layout planning of floating offshore wind farms, Int. J. Elec. Power, 131, 107128, https://doi.org/10.1016/j.ijepes.2021.107128, 2021.

Lozon, E., Lekkala, M. R., Sirkis, L., and Hall, M.: Reference mooring and dynamic cable designs for representative U.S. floating wind farms, Ocean Eng., 322, 120473, https://doi.org/10.1016/j.oceaneng.2025.120473, 2025.

Mahfouz, M. Y.: D1.3. Public design and FAST models of the two 15MW floater-turbine concepts, Tech. rep., COREWIND http://corewind.eu/publications/ (last access: 5 February 2026), 2020.

Mahfouz, M. Y., Lozon, E., Hall, M., and Cheng, P. W.: Integrated floating wind farm layout design and mooring system optimiza-

tion to increase annual energy production, J. Phys. Conf. Ser., 2767, https://doi.org/10.1088/1742-6596/2767/6/062020, 2024.

Musial, W., MacDonald, S., Fuchs, R., Zuckerman, G. R., Carron, S., Hall, M., Mulas Hernando, D., Sathish, S., and Fan, K.: Considerations for Floating Wind Energy Development in the Gulf of Maine, Tech. Rep. NREL/TP-5000-86550, National Renewable Energy Laboratory (NREL), Golden, CO (United States), https://www.osti.gov/biblio/1989642 (last access: 5 February 2026), 2023.

Prim, R.: Shortest Connection Networks and Some Generalizations, Bell Syst. Tech. J., 36, https://doi.org/10.1002/j.1538-7305.1957.tb01515.x, 1957.

Quoceant: Moorings & Connection Systems Cost Metrics, Tech. Rep. SEC-D-012 C2, Wave Energy Scotland, https://www.waveenergyscotland.co.uk/media/ablhmxr4/sec-d-012_deliverable-3c_moorings-cost-metric.pdf (last access: 5 February 2026), 2016.

Rapha, J. I.: Floating offshore wind farm layout optimisation, Zenodo, https://doi.org/10.5281/zenodo.8328029, 2023.

Robertson, A., Jonkman, J., Masciola, M., Song, H., Goupee, A., Coulling, A., and Luan, C.: Definition of the Semisubmersible Floating System for Phase II of OC4, National Renewable Energy Laboratory (NREL), Golden, CO (United States), Tech. Rep. NREL/TP-5000-60601, 1155123, https://doi.org/10.2172/1155123, 2014.

Silva de Souza, C. E., Berthelsen, P. A., Eliassen, L., Bachynski, E. E., Engebretsen, E., and Haslum, H.: Definition of the INO WINDMOOR 12 MW base case floating wind turbine, SINTEF Ocean, ISBN 978-82-7174-407-6, https://sintef.brage.unit.no/sintef-xmlui/handle/11250/2723188 (last access: 10 October 2025), 2021.

Sirkis, L., Biglu, M., Hall, M., Moreno, F., Housner, S., and Lozon, E.: Floating Offshore Wind Farm Array Optimization Considering Mooring Lines, Anchors, and Array Cables, OnePetro, https://doi.org/10.4043/35814-MS, 2025.

Sirkis, L. H., Lozon, E., and Hall, M.: Reference Floating Wind Array Designs Dataset for Three Representative Regions, Zenodo [data set], https://doi.org/10.5281/zenodo.19055044, 2026.

Thomas, J. J., Baker, N. F., Malisani, P., Quaeghebeur, E., Sanchez Perez-Moreno, S., Jasa, J., Bay, C., Tilli, F., Bieniek, D., Robinson, N., Stanley, A. P. J., Holt, W., and Ning, A.: A comparison of eight optimization methods applied to a wind farm layout optimization problem, Wind Energ. Sci., 8, 865–891, https://doi.org/10.5194/wes-8-865-2023, 2023.

United States Department of Homeland Security and United States Coast Guard: CH-1 to Navigation and Vessel Inspection Circular (NVIC) 02-23, Tech. rep., United States Coast Guard, https://www.dco.uscg.mil/Portals/9/OCSNCOE/References/NVICs/NVIC-02-23-CH1.pdf?ver=eUc99J4wHcSjb7w38uaqZQ== (last access: 6 January 2025), 2024.

van Koten, K.: Design of a suction pile multiline anchor system for floating offshore wind turbines, PhD thesis, Technical University Delft, https://resolver.tudelft.nl/uuid:992f5413-6867-435b-83d4-be6d313e3cdd (last access: 21 April 2026), 2021.

Yu, W., Muller, K., and Lemmer, F.: Qualification of innovative floating substructures for 10MW wind turbines and water depths greater than 50m: Deliverable D4.2 Public Definition of the Two LIFES50+ 10MW Floater Concepts, Tech. rep., LIFES50+, https://doi.org/10.3030/640741, 2018.

Zahle, F., Barlas, T., Lonbaek, K., Bortolotti, P., Zalkind, D., Wang, L., Labuschagne, C., Sethuraman, L., and Barter, G.: Definition of the IEA Wind 22-Megawatt Offshore Reference Wind Turbine: IEA Wind TCP Task 55, Technical University of Denmark, https://doi.org/10.11581/DTU.00000317, 2024.